Reviewed research article

Seismic signatures of the 2015–2021 Skaftárkatlar jökulhlaups

Bethany E. Vanderhoof[1], Kristin Jónsdóttir[1], Bryndís Brandsdóttir[2], Ólafur Gudmundsson[3,2], Bergur Einarsson[1], Jean Soubestre[1,4], Ka Lok Li[5], Eyjólfur Magnússon[2] and Tom Winder[2,6]

[1]*Icelandic Meteorological Office (IMO), Bústaðavegur 7–9, IS-105 Reykjavík, Iceland*

[2]*Institute of Earth Sciences, Science Institute, University of Iceland, Reykjavík, Iceland*

[3]*Department of Earth Sciences, Uppsala University, Uppsala, Sweden*

[4]*Université Grenoble Alpes, Université Savoie Mont Blanc, CNRS, IRD, Université Gustave Eiffel, ISTerre, Grenoble, France*

[5]*Geophysics Section, School of Cosmic Physics, Dublin Institute for Advanced Studies, Dublin, Ireland*

[6]*Bullard Laboratories, Department of Earth Sciences, Cambridge University, Cambridge, United Kingdom*

Corresponding author bethanyva@vedur.is; https://doi.org/10.33799/jokull2025.75.055

Abstract — *The Skaftá cauldrons, a pair of surface depressions NW of Grímsvötn on the Vatnajökull glacier, signify subglacial lakes created by geothermal heat sources within the underlying bedrock. These subglacial lakes continuously grow in volume and each produce jökulhlaups every 1–5 years at the glacier outlet 35–40 km away. Seismic activity associated with the eight 2015-2021 jökulhlaups from the Skaftá cauldrons was analyzed, reflecting striking similarities. Seismic activity associated with subglacial flood propagation and cauldron deepening was dominated by small transient signals, interpreted as icequakes from ice deformation and hydrofracturing as the water starts to migrate subglacially. Low-amplitude, low-frequency highly repetitive events were discovered during this period for the larger magnitude jökulhlaups, possibly relating to stick-slip motion of the glacier at the bedrock. Seismic tremor events coincide with these large floods, but the origin of the tremor has been disputed. Sustained tremor (1–3 Hz) persists for 1.5–3 days, while high-amplitude tremor bursts (0.5–4 Hz) with durations up to tens of minutes and a strong relationship with increased electrical conductivity in the flood water are observed once most of the water has drained from the cauldrons, exhibiting higher amplitudes during larger jökulhlaups. A probabilistic location method reveals that this 0.5–4 Hz tremor is co-located with the cauldrons and temporally coincides with the end of cauldron subsidence, indicating that the tremor is related to the rapid depressurization of the bedrock and is likely generated by either confined shallow level magmatic activity or enhanced geothermal activity such as vigorous boiling or hydrothermal explosions.*

INTRODUCTION

The southeast coast of Iceland is frequently impacted by jökulhlaups (glacial outburst floods) from the Vatnajökull ice cap that flow into glacial rivers, posing significant risks to infrastructure and farmlands within the glacier outwash plain. These floods typically originate from subglacial lakes formed by the high-temperature geothermal areas that are associated with central volcanoes, where shallow magmatic or eruptive activity can exacerbate the hazards (Björnsson and Einarsson, 1990; Björnsson, 2003). The Skaftá cauldrons, two large depressions in the 400–500 m-thick glacier of NW-Vatnajökull (Figure 1), are each the source of fast-rising jökulhlaups every 1–5 years (Guðmundsson *et al.*, 2018). The cauldrons, which are 2–3 km wide and 50–150 meters deep, are surrounded by major crevasses and overlie semi-stable subglacial lakes that are created and maintained by geothermal heat sources in the underlying bedrock, with a combined power exceeding 1 GW

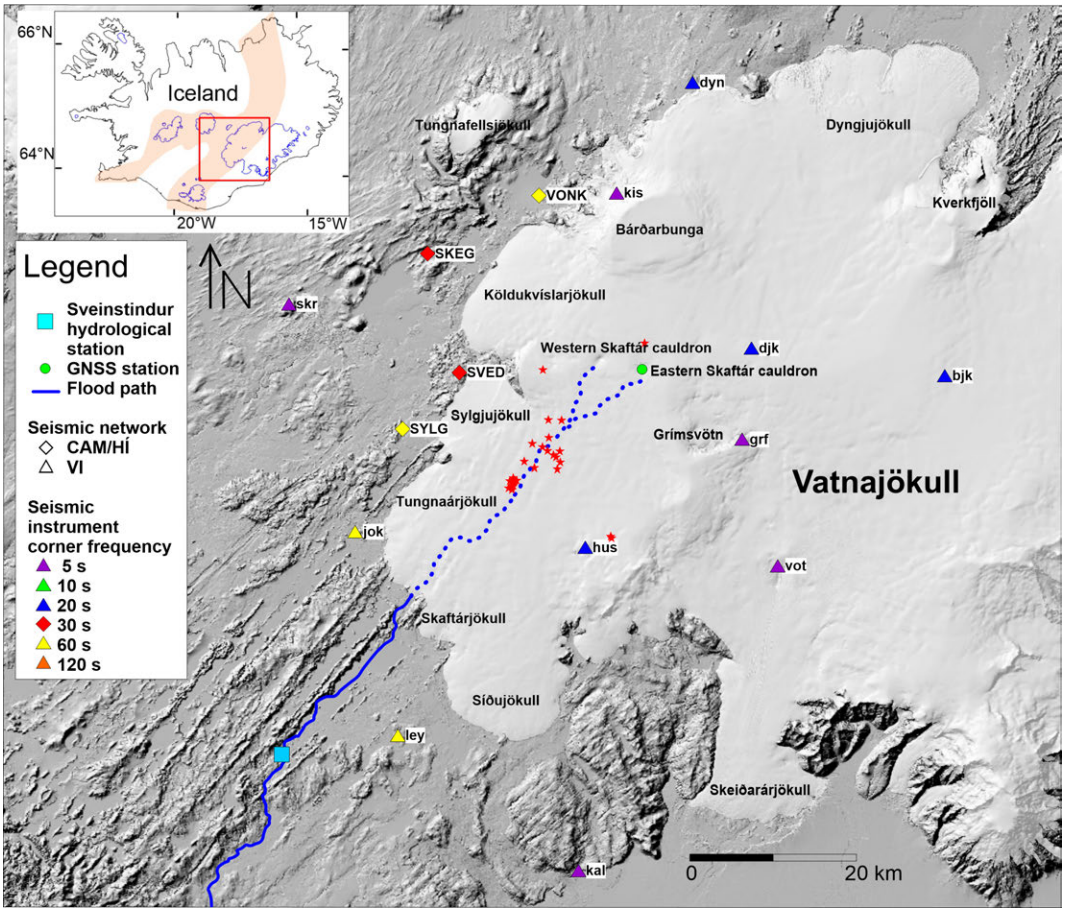

Figure 1. Map of western Vatnajökull, SE Iceland (inset), showing seismic stations, color-coded by instrument type, the Sveinstindur hydrological station, and GNSS station within the Eastern cauldron in August 2018. The jökulhlaup pathway from the Skaftá cauldrons is shown in blue. Red stars mark Quake Migrate locations of low-frequency, repetitive events during the August 2018 jökulhlaup (Winder *et al.*, 2021). Also shown are large central volcanoes, Grímsvötn, Bárðarbunga, and Kverkfjöll. – *Kort af vesturhluta Vatnajökuls og nágrennis sem sýnir staðsetningu Skaftárkatlanna, ásamt afrennsliseiðum frá þeim undir jökli, niður í Skaftá. Jarðskjálftamælistöðvar Veðurstofu Íslands (VÍ), Cambridgeháskóla (CAM) og Jarðvísindastofnunar Háskólans (HÍ) eru merktar á kortið, einnig staðsetning GPS mælitækis VÍ í eystri Skaftárkatlinum í hlaupunum 2015E, 2018EW og 2021WE og vatnshæðarmælis við Sveinstind. Rauðar stjörnur sýna staðsetningu jarðskjálfta sem fylgdu hlaupinu úr eystri katlinum, 1–5, ágúst 2018.*

(Björnsson, 2003; Guðmundsson *et al.*, 2018). The volume of these subglacial lakes increases steadily as the surrounding ice melts, comprising 71% of total inflow (Jóhannesson *et al.*, 2007). Radio-echo soundings indicate that lake geometry fluctuates over time due to changes in geothermal heat distribution, creating a thinner ice shelf in areas overlying bedrock with higher heat flow (Magnússon *et al.*, 2021). The term 'ice shelf' is here used to refer to ice that is supported by flotation over the subglacial lakes, as defined by Einarsson *et al.* (2017), not as ice shelves overlying ocean water at the margins of a glacier. Since their discovery in the mid-20th century, the Skaftá cauldrons have expanded, exhibiting a slow trend towards increasing geothermal power (Björnsson, 2003; Gudmundsson *et al.*, 2018).

Jökulhlaups from the Skaftá cauldrons (Skaftárhlaups) occur when water accumulates in the subglacial lakes, causing an increase in pressure that eventually breaks the subglacial seal at the lake margins and initiates a flood. Between 1955 and 2021, fifty-seven Skaftárhlaups have been observed, typically rising to peak discharge within 1–3 days and receding over 1–2 weeks (Guðmundsson *et al.*, 2018). These fast-rising jökulhlaups travel 35–40 km beneath the glacier in 29–62 hours (Figure 1; Einarsson *et al.*, 2017), propagating via a subglacial pressure wave that rapidly lifts the glacial ice, allowing floodwater to flow as a sheet beneath the glacier before it consolidates into tunnel-like conduits as the flood progresses with time, evidenced by GNSS data (Einarsson *et al.*, 2016, 2017; Magnússon *et al.*, 2007). Although the lakes drain significantly (Magnússon *et al.*, 2021), they do not drain completely, so large parts of the ice shelf should never be in direct contact with the bedrock (Einarsson *et al.*, 2017). It should be noted that Einarsson *et al.* (2016) suggest some jökulhlaups originating from the western cauldron appear to be an intermediary between fast- and slow-rising jökulhlaups.

Jökulhlaups from the Skaftá cauldrons emerge from Skaftárjökull and typically flow into the western branch of the Skaftá river, Eldvatn by Ásar, though water occasionally diverts to Hverfisfljót and Djúpá (Björnsson, 1988; Einarsson, 2009). The floods transport geothermal gases including CO_2 and toxic levels of H_2S from the cauldrons, with most degassing occurring within 3 km of the glacier margin (Galeczka *et al.*, 2015). During these events, dissolved and suspended materials in the floodwater increase significantly both near the glacier outlet and downstream into the lowlands (Zóphóníasson and Pálsson, 1996).

Tracking the progression of jökulhlaups is essential for natural hazards monitoring at the Icelandic Meteorological Office (IMO), as it enables monitoring personnel to identify events quickly and respond effectively. While GNSS and hydrologic measurements help to identify these floods, real-time seismic data is critical for early warnings, forming the backbone of the 24/7 operational monitoring system. Skaftárhlaups produce characteristic seismic activity, consisting of low-amplitude seismicity during subglacial floodwater propagation and high-amplitude tremor after most water has drained from the cauldrons (e.g. Björnsson and Einarsson, 1990; Einarsson *et al.*, 1997; Einarsson, 2018; Eibl *et al.*, 2020, 2023). The seismic activity associated with the 2015-2021 Skaftárhlaups was analyzed in conjunction with GNSS and hydrologic data and linked to specific physical processes, resulting in a detailed overview of what to expect during a Skaftárhlaup, thereby enhancing the monitoring team's capacity to assess data during an ongoing jökulhlaup.

DATA AND METHODS

Data

Twelve IMO seismic stations located within a 70 km radius of the Skaftá cauldrons (Figure 1), including two stations within the glacial ice (DJK and BJK), were the primary source of data for this study. Two Cambridge University/University of Iceland operated stations at the western margin of the glacier were also included. The seismic network is hampered by a lack of suitable places for station installations, as nunataks in the glacier and bedrock outcrops on the outwash planes are scarce. The seismometers, which include instrument types with a flat response for frequencies ranging from 5–120 seconds, were configured to record continuous data at a rate of 100 samples per second. The seismic data were analyzed and interpreted in conjunction with hydrologic and geodetic data with regard to flood-water propagation and cauldron subsidence.

Hydrological measurements from the IMO gauging station Sveinstindur, located on the Skaftá river 25 km downstream from the glacier margin and $\sim$65 km from the cauldrons (Figure 1), include conductivity, water temperature, and flow rate calculated from river height, collected with a temporal resolution of five minutes. There is a several-hour delay between the emergence of floodwater at the glacier margin and its arrival at Sveinstindur; typically, the travel time of the initial flood wave is approximately 7 hours during smaller jökulhlaups, but it can be as low as 3 hours for particularly large jökulhlaups (Einarsson, 2009).

It should be noted that, during Skaftárhlaups, Sveinstindur measures proglacial discharge from the flood in addition to typical runoff from the glacier and several small tributaries, which contribute an average discharge on the order of 100 m^3/s at Sveinstindur (Einarsson, 2009; Einarsson *et al.*, 2017).

A semi-permanent IMO-GNSS station, located near the center of the eastern Skaftá cauldron, has provided continuous elevation data since 2014. Subsidence curves for jökulhlaups from the eastern cauldron in 2015, 2018, and 2021 were recorded, but the total elevation drop does not necessarily indicate the maximum and minimum cauldron elevations, as the station is offset from the location of maximum subsidence. Thus, additional cauldron elevation data acquired by a combination of GNSS profile and radar altimeter campaigns were provided by Guðmundsson *et al.* (2018) spanning the 2015–2019 jökulhlaups. Cauldron subsidence for the 2021 jökulhlaups was derived from digital elevation maps (DEMS) based on SPOT7 satellite data and oblique aerial photographs.

Methods

Joint analyses and interpretation of seismic, hydrological, and geodetic data was fundamental for constructing a comprehensive overview of the activity during each jökulhlaup.

Real-time seismic amplitude measurements (RSAM) were calculated for seismic stations within 70 km of the cauldrons to quantify variations in seismic energy over the course of each jökulhlaup. RSAM was developed to address the specific issue of monitoring seismic activity when individual events are difficult to identify (Murray and Endo, 1989). The RSAM methodology downsamples the seismic data by calculating and plotting the average absolute amplitude of a signal, traditionally over 1 or 10 minutes, in order to visualize long-term changes over many hours or days of data. Different earth processes may be preferentially associated with different frequencies, so bandpass filters (0.5–1 Hz, 1–2 Hz, and 2–4 Hz) were applied to the three-component seismic data before averaging the data in one minute segments in order to enhance signals within each frequency range. Each data point is an average amplitude measurement in m/s.

The cumulative amplitude spectral density was also computed over the frequency bands 0.5–1.0, 1.0–2.0, 2.0–4.0, and 4.0–8.0 Hz. These plots display the square root of the integrated power-spectral density. For a common seismic trace, the resulting curves are qualitatively the same as RSAM, but calculating the strength of a signal in the given frequency bands is more efficient using the cumulative amplitude spectral density.

The network processing python package covseisnet (https://github.com/covseisnet) was used to analyze the phase coherence (i.e. spatial coherence) of the seismic wavefield recorded over the region, as described by Seydoux *et al.* (2016) and Soubestre *et al.* (2018). Phase coherence is represented by the network covariance matrix spectral width. A low spectral width value indicates strong signal coherency across the network at a given time and frequency. The spectral width of the wavefield recorded by the network was calculated at each frequency and each time window of 100 seconds for the duration of each Skaftárhlaup. Between eight and eleven stations were used in each analysis, revealing tremor and transient signals observed across the western Vatnajökull seismic network. The initial analyses were conducted from 0.01 Hz to 50 Hz (Nyquist frequency), but subsequent spectral width plots were focused up to 10 Hz, below which most of the coherent tremor signals are visible.

Spectral and waveform analyses were utilized to further characterize the spectral content, amplitude, and shape of the seismic waveform data during Skaftárhlaups. To investigate tremor, transient signals were suppressed in spectrograms to enhance weaker tremor. Spectrograms were computed up to 50 Hz, but since notable tremor is generally below 8 Hz, spectrograms were truncated at this maximum value.

Strong (i.e. high-amplitude) tremor (e.g. Björnsson and Einarsson, 1990; Einarsson *et al.*, 1997; Einarsson, 2018; Eibl *et al.*, 2020, 2023) was located using the probabilistic tremor location method of Li and Gudmundsson (2020). This method calculates cross-correlation envelopes for each pair of seismic stations, using Bayes theorem to map each envelope to a probability density as a function of time shift. The time series of each pair is back-projected to obtain a probabil-

ity density of the most likely source location in space. The joint-likelihood of locations for all station pairs is subsequently calculated as the product of the individual station pair probabilities. The resulting probability distribution has a peak at the most likely location of the dominant source during a given time period. This method was used to locate 0.5-4.0 Hz tremor in 2D space, using a uniform velocity model with a Rayleigh-wave group velocity of 1.1 km/s, similar to velocities measured at Katla (Scattoni *et al.*, 2017) and Eyjafjallajökull (Benediktsdóttir *et al.*, 2017).

OVERVIEW OF THE 2015–2021 SKAFTÁRHLAUPS

For simplicity, individual jökulhlaups will be referred to by the year of the jökulhlaup and the cauldron that drained. Thus, a jökulhlaup from the western cauldron in 2015 is abbreviated as "2015W," while jökulhlaups that occurred within several days from the eastern and then western cauldron in 2018 are referred to as "2018EW."

Eight jökulhlaups occurred between 2015 and 2021, of which five originated within the eastern Skaftá cauldron and three in the western cauldron. Each of these Skaftárhlaups began between June and September, coinciding with the increasing summer melt from Vatnajökull glacier. Seven of these Skaftárhlaups were fast-rising, reaching maximum discharge in 1 to 2 days, whereas the 2019W jökulhlaup exhibits intermediate behavior, rising to maximum discharge in approximately 9 days.

The 2015E, 2018EW, and 2021WE jökulhlaups, exhibited maximum discharges into the Skaftá river of $\sim$3000 m^3/s, 1900 m^3/s and 1350 m^3/s, respectively (Table 1). The eastern and western cauldrons drained within a day of each other during the 2018EW jökulhlaup, so the discharge and volume estimates cannot be distinguished between cauldrons. The cauldrons drained within one week of each other during the 2021WE jökulhlaup, resulting in similar limitations. The western cauldron produced the three additional small 2015W, 2016W, and 2019W jökulhlaups, which displayed small maximum discharges, 280 m^3/s or less, an order of magnitude smaller than during the large jökulhlaups. A rough, positive correlation exists between maximum discharge rate, volume drained, and cauldron subsidence for most jökulhlaups. The 2019W jökulhlaup is an outlier, having both a low maximum discharge rate and high volume of water that drained from the cauldron. During this event, 118 GL of water drained from the western cauldron (Gunnar Sigurðsson, pers. comm., Table 1), which is a similar volume to that drained during large jökulhlaups from the eastern cauldron.

The highest RSAM of 6.67×10^{-4} m/s was recorded during the 2018EW jökulhlaup, at station VONK, which is 24 km from the eastern cauldron and 21 km from the western cauldron. These RSAM values corresponded with the most significant subsidence values, as well as the maximum volume and electrical conductivity, for both cauldrons between 2015 and 2021; 128 m for the western cauldron and 129 m for the eastern cauldron (Table 1). The 2015E, 2019W, and 2021WE jökulhlaups also have maximum RSAM amplitudes on the order of 10^{-4} m/s, measuring 1.38×10^{-4} m/s, 1.05×10^{-4} m/s, and 1.29×10^{-4} m/s, respectively. Maximum amplitudes during the small 2015W and 2016W jökulhlaups are on the order of 10^{-6} m/s and 10^{-5} m/s, an order of magnitude lower. A positive correlation exists between the maximum RSAM amplitude, maximum electrical conductivity, and maximum discharge (Figure 2).

RESULTS

Temporal evolution of seismic activity, ice subsidence, discharge, and electrical conductivity

The general progression of a typical fast-rising jökulhlaup from the eastern Skaftá cauldron in terms of small transient seismic activity, low-frequency events and tremor, cauldron subsidence and hydrologic measurements is similar (Figure 3). Exceptions and variations to this general timeline most frequently arise during smaller jökulhlaups from the western cauldron. Based on the large 2015E, 2018EW (Figure 4), and 2021WE jökulhlaups, a typical jökulhlaup from the eastern Skaftá cauldron will proceed as follows:

Days 0–1: Small transient signals appear in the seismic record, with the activity gradually increasing and continuing until day 4 (Figure 4d,e). Most of these signals are very low-amplitude and do not exhibit

Table 1. The main parameters of the 2015–2021 jökulhlaups. The start dates of the jökulhlaups are based on the small transient seismic signals detected at near-field stations (Figure 3), which begin 1–3 days earlier than flood waters reach the Sveinstindur hydrological gauging station. Variables including total volume drained from the cauldron, maximum electrical conductivity, and maximum discharge are shared between jökulhlaups that start too close in time (the 2018EW jökulhlaups and 2021WE jökulhlaups). ⋆ There is no continuous seismic data during the start of the 2015W jökulhlaup, so the start date is based on the time of flood water arrival at Sveinstindur. ⋆⋆ The start date of the 2018 jökulhlaup from the western cauldron is estimated, as this flood directly overlaps with the jökulhlaup from the eastern cauldron. – *Yfirlit yfir sig, hámark skjálftaóróa, hlaupstærð, leiðni og hámarksrennsli jökulhlaupanna 2015–2021. Þar sem GPS-gögn eru ekki til staðar er upphaf jökulhlaupanna miðað við ísskjálfta sem koma fram á jarðskjálftamælum næst kötlunum (sjá 3. mynd), 1–3 dögum áður en hlaupvatn mælist á vatnshæðarmælistöðinni í Skaftá, við Sveinstind. Þegar hlaupin úr kötlunum skarast er illmögulegt að aðgreina rúmmál, rafleiðni og hámarksrennsli á milli þeirra, þetta eru jökulhlaupin 2018EW og jökulhlaupin 2021WE. ⋆Engin samfelld jarðskjálftagögn eru til af upphafi jökulhlaupsins úr vesturkatlinum í júní, 2015W, dagsetningin miðast því við tímann sem flóðvatnið kom fram við Sveinstind. ⋆⋆ Upphafsdagur jökulhlaupsins frá vestari katlinum 2018 er áætlaður, þar sem hlaupið kom í kjölfar hlaupsins úr eystri katlinum.*

Year	Cauldron	Start date	Cauldron subsidence [m]	Max RSAM m/s	Volume GL	Max electrical conductivity [μS/cm]	Max discharge [m^3/s]
ár	*ketill*	*hlaup hefst*	*ketilsig*	*mesta útslag*	*GL*	*leiðni*	*hámarksrennsli*
2015	West	2015-06-16*	100	9.87 E-6	∼90	302	210
2015	East	2015-09-27	111	1.38 E-4	∼402	519	∼3000
2016	West	2016-09-05	86	2.43 E-5	∼130	180	250
	East	2018-07-30	129				
2018				6.67 E-4	∼437	603	1900
	West	2018-07-31**	128				
2019	West	2019-09-12	71	1.05 E-4	∼118	305	280
	West	2021-08-28	94	1.29 E-4		533	
2021					∼404		1350
	East	2021-09-05	104	6.30 E-5		380	

phase coherence across the western Vatnajökull seismic network. Many of these events are locatable by the permanent seismic network and listed in the IMO catalogue. Eibl *et al.*, (2023) located 45 events during the 2015E jökulhlaup of which 21 were automatically detected by the SIL network. About twenty events were located by the SIL network during the first four days of the August 2018E jökulhlaup.

Day 2: Gradual subsidence of the cauldron begins, lowering 6–8 m in 24–36 hours (Figure 4a).

Day 3: Repetitive, low-frequency (0.5—3 Hz) signals appear in the seismic record and continue intermittently for 24 hours or more. These events may be used to separate jökulhlaups between cauldrons (Figure 4d.) Discharge begins to increase at Sveinstindur, rising to its maximum value in 12–36 hours (Figure 4c). Electrical conductivity increases at Sveinstindur with the arriving flood wave, rising in less than 12 hours and remaining at its maximum level for the next 1.5 days (Figure 4b). The cauldron undergoes its most drastic period of subsidence on this day, falling 40–100 m in 24 hours.

Day 4: Strong seismic tremor consisting of sustained tremor (1–3 Hz) and tremor bursts (0.5–4 Hz) begins and continues for 1.5 to 3 days (Figures 4d,e and 5). The cauldron enters its final phase of subsidence, losing an additional 10–20 m of elevation over 2 days, ending on day 6. The discharge at Sveinstindur starts to recede, typically falling within 2–7 days.

Day 5: A secondary increase in electrical conductivity begins. Once it reaches a new maximum value, increasing by 50–300 μS/cm in 6–24 hours, it starts receding immediately (Figure 4b).

Days 6–7: Tremor ceases. The flood water recedes, and discharge and conductivity levels return to normal levels.

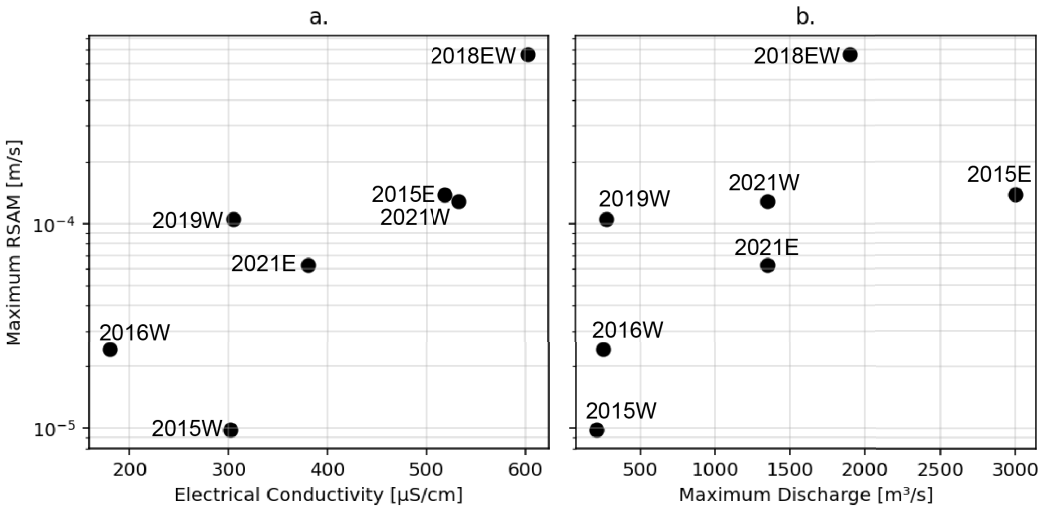

Figure 2. Maximum electrical conductivity (a) and maximum discharge (b) measured at Sveinstindur versus maximum RSAM of Phase II tremor at station VONK, for the jökulhlaups from the eastern (E) and western (W) cauldrons, listed in Table 1. – *Hámarks rafleiðni (a) og hámarksrennsli (b) jökulhlaupa samkvæmt mælingum við Sveinstind í samanburði við styrkleika skjálftaóróa (RSAM) á jarðskjálftamælinum í Vonarskarði (VONK). Jarðóróinn mælist á flestum stöðvum í seinni hluta jökulhlaupanna (fasa 2 á 3. mynd), eftir að megnið af vatninu er runnið úr kötlunum. Jökulhlaupin frá austur- (E) og vestur- (W) katlunum eru aðgreind, sjá einnig töflu 1.*

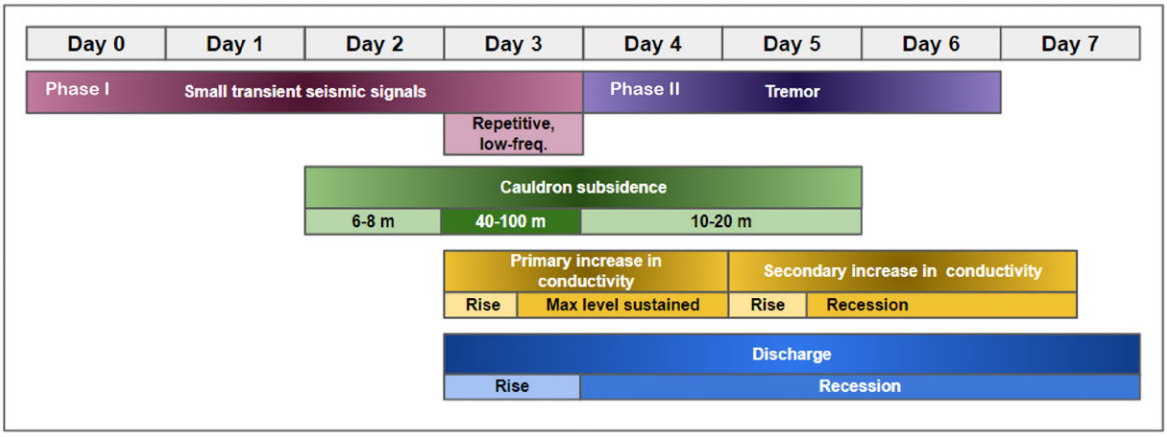

Figure 3. Timeline of Phase I and II events during a typical fast-rising Skaftárhlaup, based on jökulhlaups from the eastern cauldron in 2015, 2018, and 2021. The conductivity and discharge rows are based on data recorded at the Sveinstindur hydrological station, located approximately 60 km southwest of the cauldrons. – *Þróun atburða í jökulhlaupum úr austurkatlinum árin 2015, 2018 og 2021, sem koma fram á jarðskjálftamælum svæðisins. Skjálftagögnin skiptast í tvo fasa. Fyrri fasinn (I) einkennist af smágerðum skjálftum (ísbrestum) og litlum lágtíðniskjálftum, sem sýndir eru á 6. mynd. Seinni fasinn (II) einkennist af skjálftaóróa ásamt sterkum óróahviðum. Gögn um leiðni og rennsli eru samkvæmt vatnamælingum við Sveinstind, um það bil 60 km suðvestur af katlinum.*

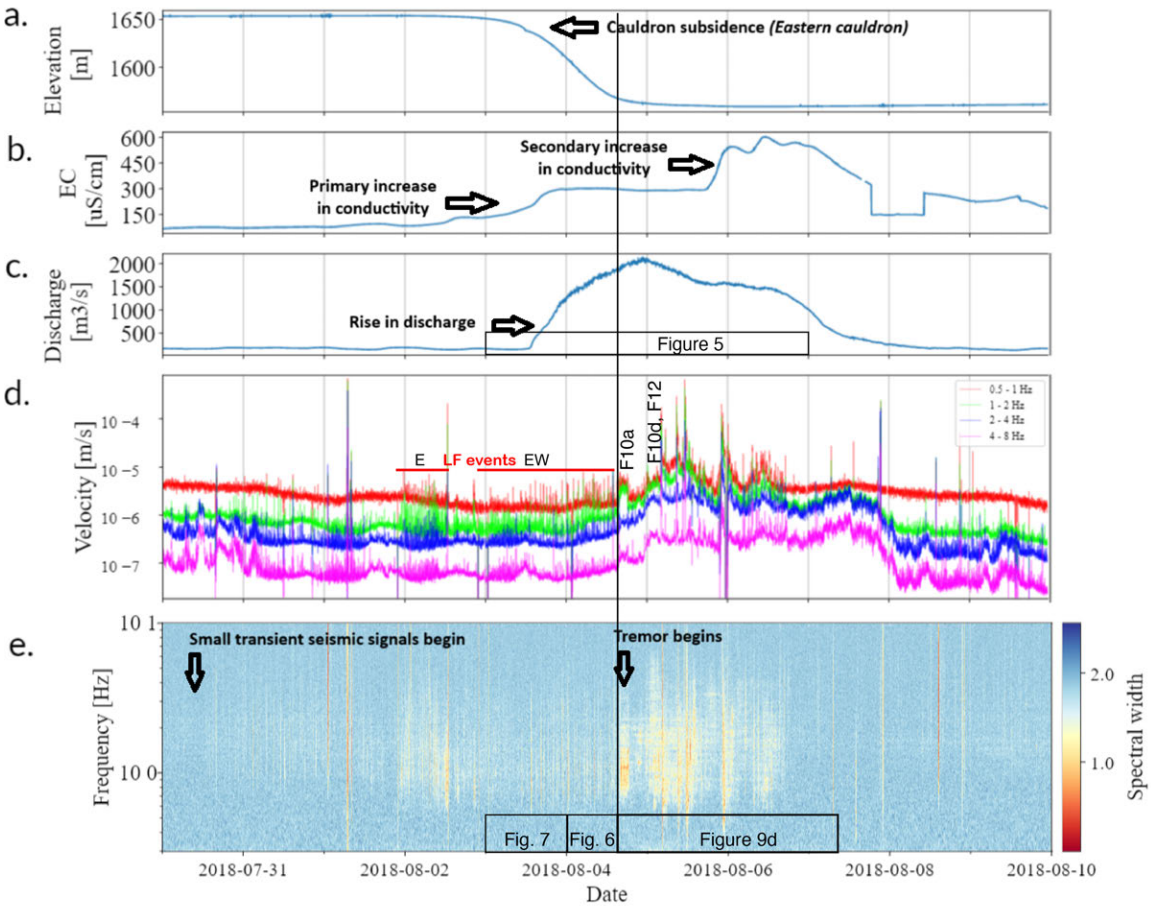

Figure 4. Overview of the July-August 2018 jökulhlaups (2018EW). Black vertical line separates Phases I and II. Boxes denote the time span of Figures 5, 6, 7 and 9d. a) Vertical subsidence curve of the GNSS station in the eastern Skaftá cauldron, b) Average electrical conductivity measured at Sveinstindur, c) Discharge measured at Sveinstindur, d) 1-minute RSAM of seismic data filtered between 0.5–1.0 Hz (red), 1.0–2.0 Hz (green), 2.0– 4.0 Hz (blue), 4.0–8.0 Hz (magenta) at station VONK, 24 km from the eastern cauldron and 21 km from the western cauldron, Location of Figures 10a, 10d and 12 is also shown. e) Network covariance matrix spectral width computed from 10 seismic stations. – *Yfirlit yfir jökulhlaupin úr báðum kötlunum 2018 (2018EW). Lóðrétta línan aðgreinir fasa I og II. Tímabil mynda 5, 6, 7 og 9d eru einnig afmörkuð. a) GPS skráning á siginu í eystri katlinum. b) Meðalrafleiðni og c) vatnsmagn við Sveinstind, d) Óróamæling, einnar mínutu meðaltal af styrkleika skjálftaóróa á tíðnibilinu 0,5–1,0 Hz (rautt), 1,0–2,0 Hz (grænt), 2,0–4,0 Hz (blátt), 4,0–8,0 Hz (lilla-blátt) á mælinum í Vonarskarði (VONK), 24 km frá austurkatlinum og 21 km frá vesturkatlinum. Staðsetning tromlurita á mynd 10a og 10d og óróahviða á 12. mynd er merkt. e) Samfylgni tíðnirófs óróahviða mæld á 10 skjálftamælistöðvum. Litaskalinn endurspeglar styrk tíðnirófsins. Óróahviðurnar ágerast þegar líður á hlaupið og ná hámarki eftir að megnið af vatninu hefur runnið frá katlinum.*

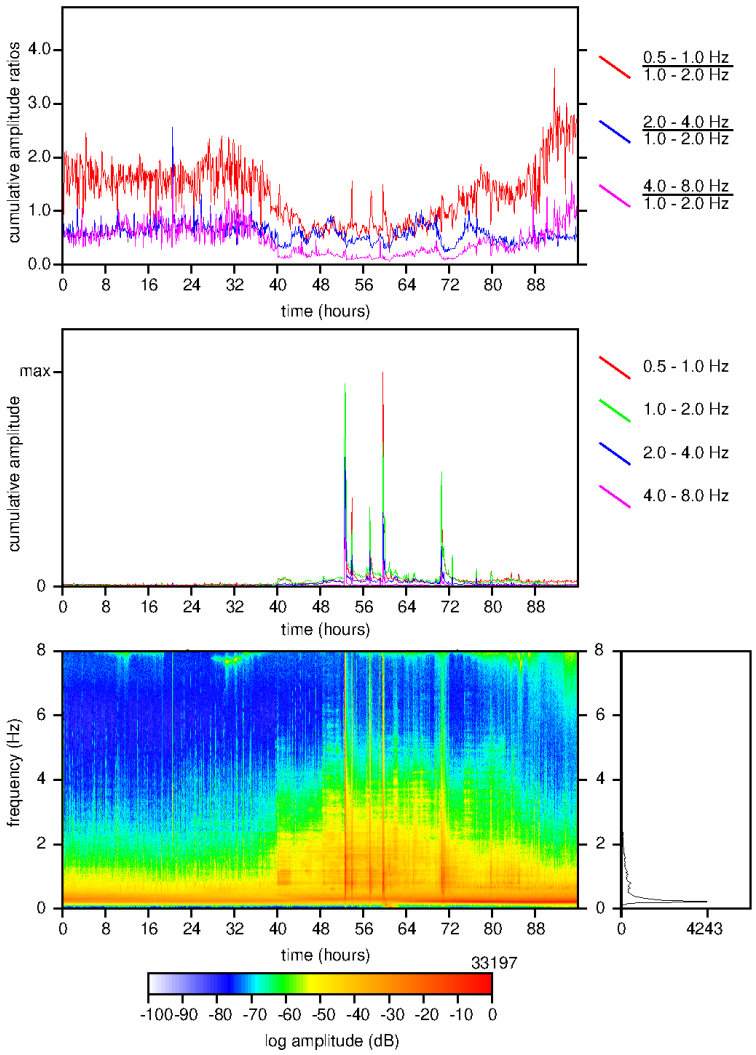

Figure 5. Four-day overview of Phase I and II seismic activity in the vertical component of station DJK during the 2018EW jökulhlaup. The time axis spans August 3–7, 2018. a) cumulative amplitude ratios, b) cumulative amplitude spectral density, and c) spectrogram with logarithmic amplitude scaling. – *Yfirlit yfir jarðskjálftavirkni 3.–7. ágúst, 2018, á mælistöðinni á Dyngjujökli (DJK) samfara jökulhlaupinu 2018EW, úr báðum kötlunum. Fyrstu tvo dagana er smáskjálftavirknin mest áberandi en síðan óróahviðurnar, sem kom fram sem lóðrétt úslög, a) styrkur tíðnihlutfalla sem fall af tíma. b) styrkur mismunandi tíðna sem fall af tíma. c) Tíðnirit sem endurspeglar hvernig órói á lægri tíðnum eykst með tíma.*

Based on this general timeline, Phase I of the jökulhlaup consists of the creation of the subglacial flood path and the period of maximum cauldron deepening, spanning days 0–4 in Figure 3. In reality, this phase can last as little as four days for rapidly-rising jökulhlaups from the eastern cauldron (e.g. Figure 4) or exceed a week for intermediately-rising jökulhlaups from the western cauldron. Phase II of a Skaftárhlaup begins once most water has drained from the subglacial lake and the cauldron surface subsidence is nearly complete, although final water propagation and cauldron subsidence will occur during this time. These two phases can be characterized by the seismic activity that arises, with Phase I being dominated by transient seismic signals and Phase II being dominated by strong (0.5–4 Hz) seismic tremor.

The secondary increase in conductivity (2018-08-06 in Figure 4b) is observed approximately 24–36 hours after strong tremor begins at the cauldrons (2018-08-04 in Figure 4e). Water can travel from the cauldrons to Sveinstindur in this amount of time once the subglacial flood path has been created, so 1) the timing and 2) the positive correlation between the height of the secondary spike in conductivity and

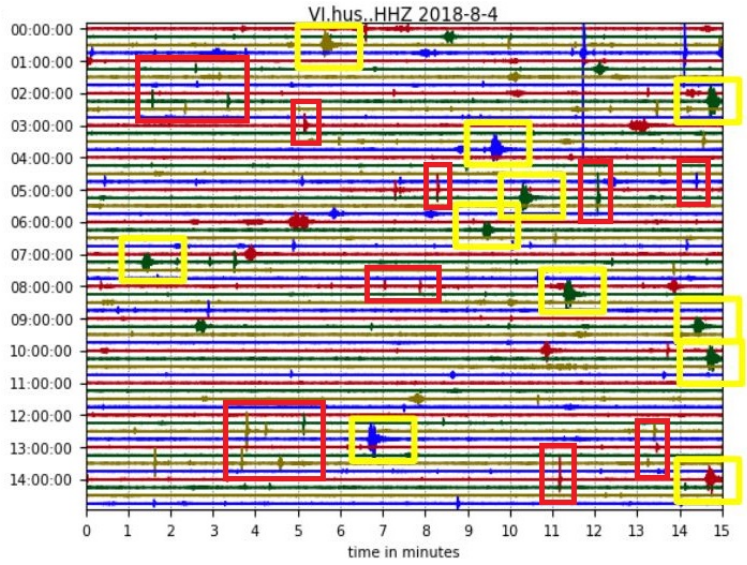

Figure 6. Drumplot showing 15 h of the vertical component of seismic station HUS (Figure 1). Phase I seismic activity on August 4, during the 2018EW jökulhlaup, filtered from 0.5–10 Hz, exhibiting small transient signals (red boxes) and repetitive, low-frequency events (yellow boxes). – *Tromlurit af 15 klst. þann 4. ágúst, 2018. Línuritið er af lóðréttra skjálftanema mælisins á jökulskerinu Húsbónda (HUS), um 20 km suðvestan Grímsvatna. Smáskjálftar (ísbrestir) og lágtíðniskjálftar í fyrri fasa 2018EW jökulhlaupsins eru afmarkaðir með rauðum og gulum ferhyrningum.*

tremor amplitude (Figure 2a) suggest that the secondary spike in electrical conductivity is directly related to the strong tremor.

Phase I Activity: During subglacial flood propagation and cauldron deepening

During the early days of a Skaftárhlaup, transient signals dominate the seismic record (Figure 6). Two distinct classes of transient signals occur during this Phase I of the jökulhlaup: 1) very small, brief transients that are not spatially coherent, and 2) low-frequency (0.5–3 Hz), long-duration, repetitive transient signals that exhibit phase coherence.

Small, local transient signals

Events falling into the prior category are typically of very short-duration, lasting from a fraction of a second to several seconds. They have small average seismic amplitudes on the order of 10^{-7} m/s or 10^{-6} m/s, and while some are seen coherently in the network covariance matrix plots (Figure 4e), most are only seen locally at individual stations. Therefore, the majority of these small signals are not identified as events by the IMO's SIL system (Böðvarsson *et al.*, 1999; Jakobsdóttir *et al.*, 2001; Jakobsdóttir, 2008). Those detected are located in vicinity of the cauldrons and in the region of the subglacial flow path (Eibl *et al.*, (2023). The waveforms, which are typically very simple, vary significantly between these events, and there is usually no clear arrival of a P- or S-phase. These small transients exhibit frequency contents between 1 and 14 Hz, but most seismic energy during Phase I of a Skaftárhlaup is focused below 2 Hz, as illustrated in the first 38 hours of Figure 5.

Low-frequency, repetitive events

Another class of transient signals also arises during Phase I of a jökulhlaup and is observed clearly during the 2018EW, 2019W, and 2021WE jökulhlaups. These low-frequency signals are strongest from 0.5–3 Hz and cluster in time, occurring once every 0.5–2 hours in a rhythmic pattern for 1 to 3 days. They are clearly and coherently seen across the seismic network of western Vatnajökull in spectral-width plots in the form of sharp spikes. This rhythmic activity was observed during the first two days of the 2018EW jökulhlaup, correlating in intensity with the elevated subsidence rate within the cauldron (Figures 4 and 7), with energy in the 0.5–1.0 and 1.0–2.0 Hz band on the cumulative amplitude spectral density plot.

The low-frequency events (e.g. on August 4, 2018, Figure 6) have strikingly similar waveforms, appear-

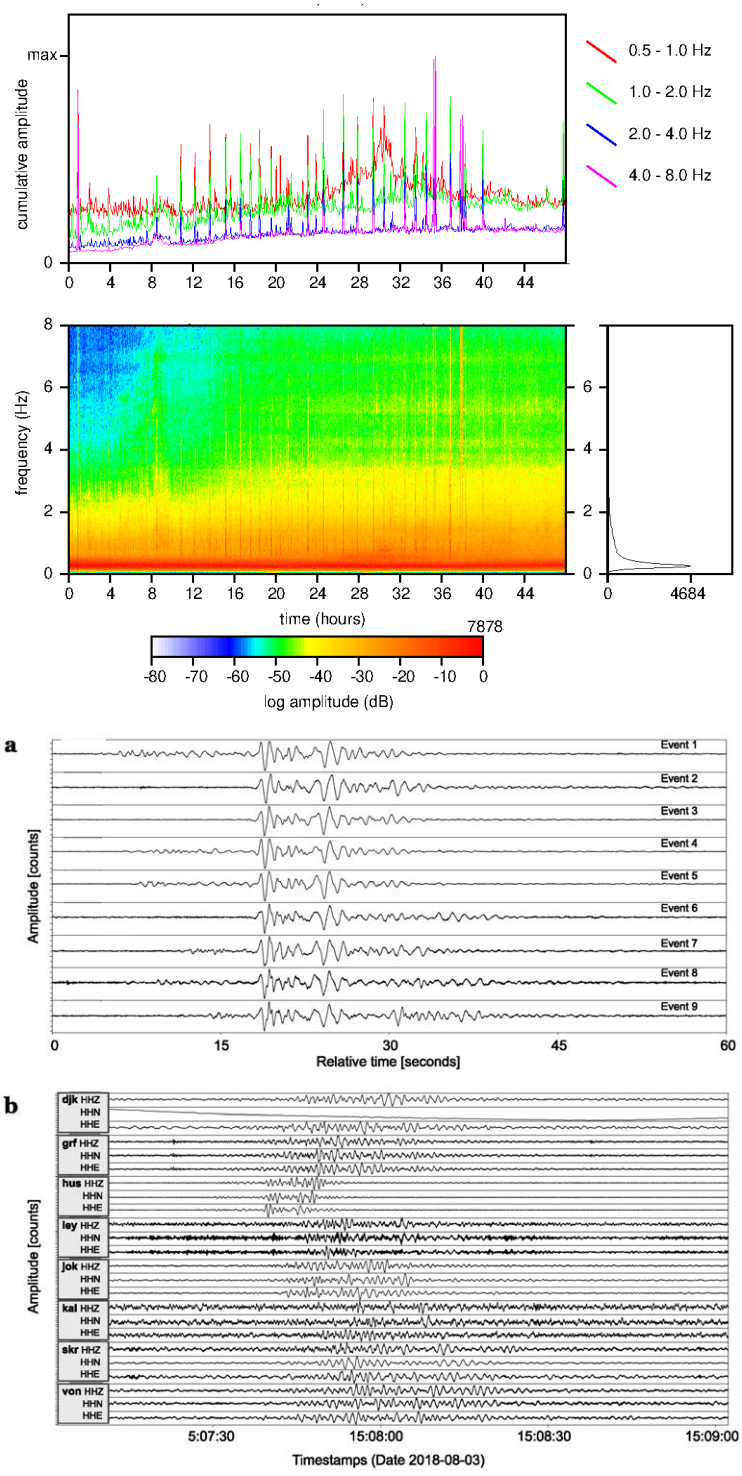

Figure 7. Spectral characteristics of the vertical component of station JOK, August 3–4, showing low-frequency, repetitive events during Phase 1 of the 2018EW jökulhlaup. (a) Cumulative amplitude spectral density and (b) spectrogram with logarithmic spectral amplitude scaling. – *Rófrit af lóðrétta nema skjálftamælisins í Jökulheimum (JOK), 3.–4. ágúst, 2018 í fyrsta fasa jökulhlaupsins 2018EW. Lágtíðniskjálftarnir koma fram sem lóðrétt útslög, Styrkur þeirra vex með tíma.* (a) styrkur mismunandi tíðnibanda sem fall af tíma. b) Tíðnirit yfir sama tímabil, styrkur rófsins er mestur undir 2 Hz.

Figure 8. Waveforms of low-frequency events during Phase I of the 2018EW jökulhlaup. (a) The east-component (station HUS) of nine repetitive, low-frequency transient signals. The top trace event at 00:35 and the lower trace to event at 02:29 in Figure 6. Traces are normalized to maximum amplitude and have been aligned to best show the similarities in their waveforms. A 0.6 Hz high-pass filter has been applied to remove low-frequency noise. (b) Three components of eight seismic stations for a single low-frequency event (August 3, 2018 at 5:07) – *Línurit af lágtíðniskjálftum í fyrsta fasa jökulhlaupsins 2018EW. (a) Níu lágtíðniskjálftar skráðir á lárétta A-V þátt mælisins á Húsbónda (HUS) á tímabilinu frá kl. 00:35 (efst) til 02:29, 3. ágúst (sjá 6. mynd). Einsleitni skjálftanna bendir til þess að orsakir/upptakahreyfingar þeirra séu þær sömu. Línuritin eru sköluð miðað við hámarks útslag hvers skjálfta til að draga betur fram hversu lík bylgjuform þeirra eru. (b) Lágtíðniskjálfti 3. ágúst 2018, kl. 05:07 skráður á átta jarðskjálftamælum.*

ing to be nearly identical at each station, indicating uniform source mechanisms and locations. The waveforms are variable between stations, reflecting heterogeneous raypaths (Figure 8). At the closest station HUS, the low-frequency events last approximately 45 seconds. However, at other stations, the duration can exceed 60 seconds. The peaks and troughs of the seismic waves align almost perfectly, although the amplitude is variable; the highest amplitudes are seen during the third and fourth events of each cluster, after which the amplitudes decay. A P-phase may be present before the impulsive, repetitive waveform that appears to be an S-phase (Figure 6), but this part of the waveform is low-amplitude, unclear, and not similar between events.

Some of the low-frequency transient signals are identified as events by the IMO's SIL/VI seismic system. The routine reviewed locations of some of these events in the SIL catalogue typically fall to the southwest of the cauldrons, roughly along the flood path. Based on the relative strong surface waves of these events, their origin is shallow, in the top few hundred to 1 km below the surface. The SIL magnitudes of these events are generally within the range 0.1–0.8. Using QuakeMigrate (Winder *et al.*, 2021), an automatic earthquake detection and location software based on waveform migration and stacking, to locate low-frequency events on August 3–4, 2018 provided well-constrained locations (Figure 1) along the flood path approximately 20 km SW of the cauldrons in good agreement with events located by SIL.

Phase II Activity: Tremor following cauldron subsidence and water drainage

Phase II of a Skaftárhlaup is characterized by strong tremor observed after most water drainage and cauldron subsidence has occurred. This activity consists of two main types of tremor: sustained tremor and tremor bursts (Figures 9 and 10).

Sustained tremor

Consistent tremor with a dominant frequency range of approximately 1–3 Hz begins once most of the water has drained from the cauldrons, exhibiting phase coherence across the seismic network in western Vatnajökull during all eight of the jökulhlaups from 2015–2021 (Figure 9). This tremor is sustained for the entire 1.5–3 day period and exhibits distinct spectral lines throughout this long-duration release of seismic energy (Figures 10 and 11). Unlike harmonic tremor, it is not composed of a fundamental frequency with overtones at consistent frequency intervals.

The multi-day sustained tremor typically initiates with a weak low-amplitude signal. For most of the jökulhlaups between 2015 and 2021, the amplitude of this early sustained tremor is on the order of 10^{-7} m/s at seismic stations close to the cauldrons. Typically, when this tremor begins, it is seen coherently across the seismic network between 1 and 3 Hz (Figure 9). Exceptions are the large 2015E and 2018EW jökulhlaups, which have a lower initial frequency content from 0.7–2 Hz. During the 2018EW jökulhlaup, a 12 hour increase of sustained tremor in the 0.5–1.0 Hz and 1.0–2.0 Hz frequency bands was initiated around midnight on August 3-4th, culminating in a particularly strong 3-4 hour long tremor burst in the morning of August 4th (Figure 7a), represented by a drastic increase in the 0.5–1.0 Hz and 1.0–2.0 Hz cumulative amplitude spectral density curves, with an amplitude on the order of 10^{-6} m/s (Figures 4 and 5).

As time progresses, the minimum and maximum frequencies of the sustained tremor evolve. The range of frequencies that exhibit phase coherence expands after several hours, typically reaching a maximum of 4 Hz for most jökulhlaups and minimum of 1 Hz for the 2015W and 2016W jökulhlaups and 0.6–0.7 Hz for the 2015E, 2018EW, 2019W, and 2021WE jökulhlaups (Figure 9). The frequency range widens midway through Phase II of the large 2015E and 2018EW jökulhlaups, with spatially coherent frequencies of sustained tremor as high as 5–6 Hz (Figures 9b and 9d). As the tremor ceases, higher frequencies typically disappear before the lower frequencies. However, it should be kept in mind that the range of frequencies exhibiting phase coherence does not necessarily represent the strongest frequencies, which are typically from 1–3 Hz.

Sustained tremor during relatively small jökulhlaups from the western Skaftá cauldron in 2015, 2016, and 2019 has a narrower frequency range and less distinct spectral lines than during large jökul-

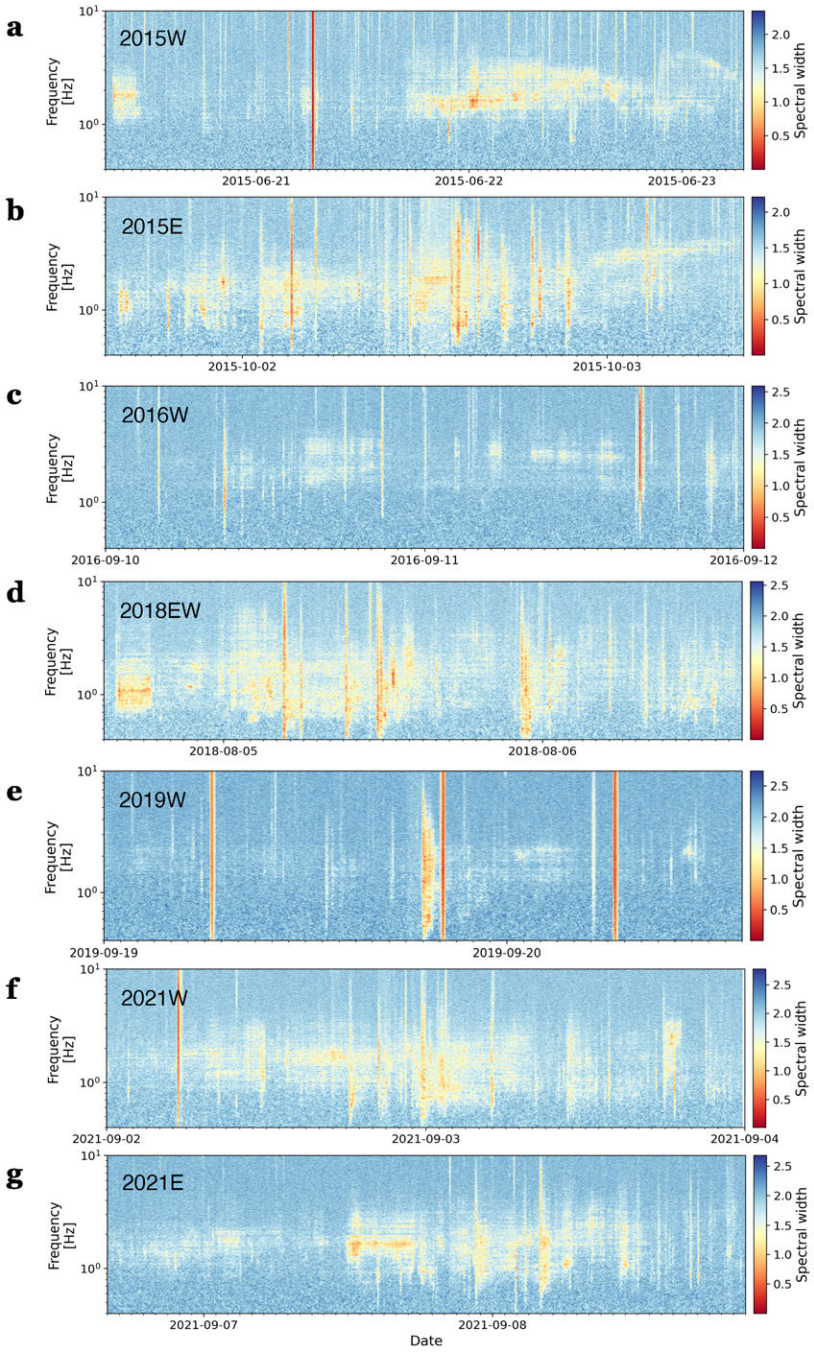

Figure 9. Network covariance matrices of tremor during Phase II, spanning the 1.5 to 3 day period of tremor after the cauldrons subside. a) 2015W, b) 2015E, c) 2016W, d) 2018EW, e) 2019W, f) 2021W, g) 2021E. – *Samfylgni óróahviða yfir 1,5 til 3 daga tímabil í seinni fasa hlaupanna, eftir að megnið af vatninu hefur runnið úr kötlunum og þeir sigið. Jökulhlaupin eru a) 2015W, b) 2015E, c) 2016W, d) 2018EW, e) 2019W, f) 2021W, og g) 2021E. Minni hlaupin 2015W, 2016W og 2019W (tafla 1) hafa færri/veikari hviður. Krafturinn í óróahviðunum virðist þannig tengjast stærð hlaupanna.*

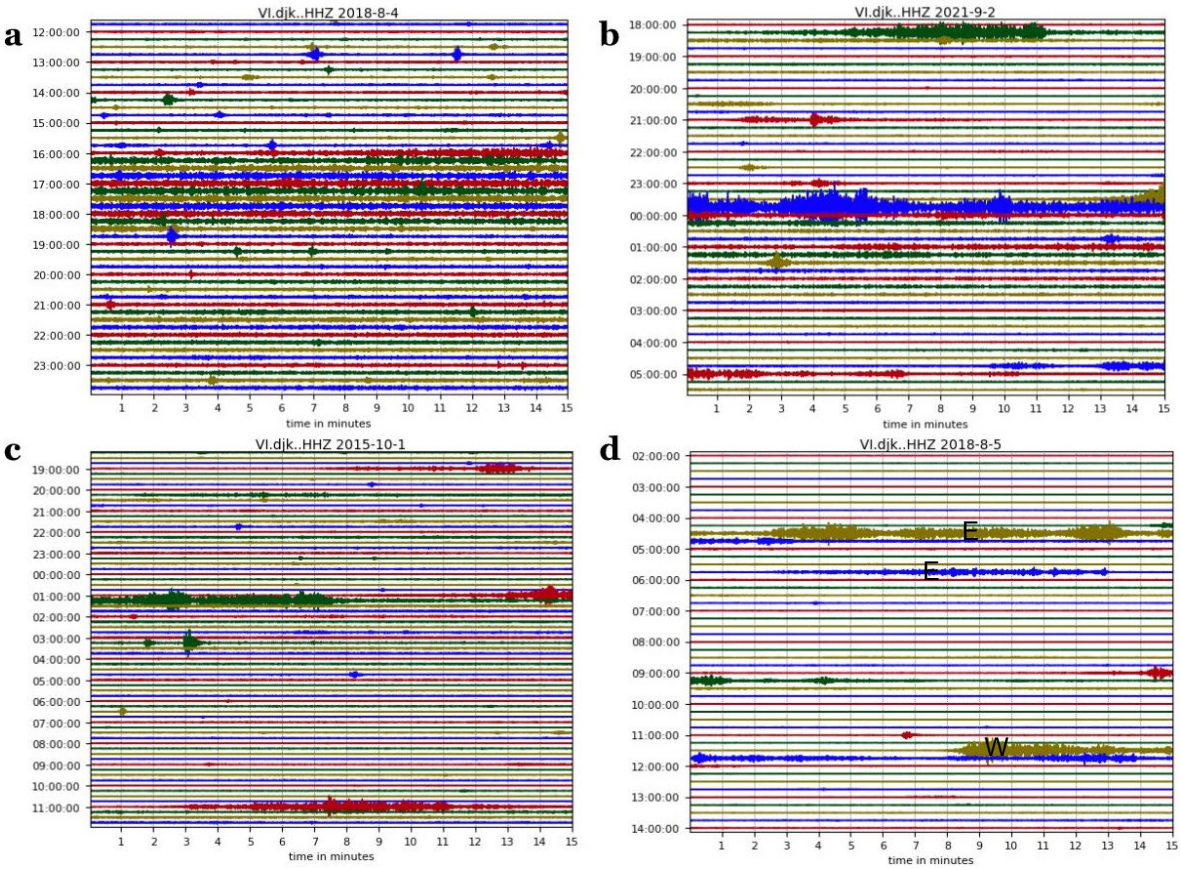

Figure 10. Drumplots of Phase II seismic activity, filtered from 0.5–4 Hz, exhibiting tremor from the Skaftárhlaups in the vertical component of DJK. a) High amplitude sustained tremor from 16:00–18:00 on August 4, during the 2018EW jökulhlaup. b) Several tremor bursts from September 2–3 during the 2021W jökulhlaup, exhibiting high-amplitude sustained tremor starting at midnight on September 3, after a large tremor burst. c) Tremor bursts from October 1–2 during the 2015E jökulhlaup, including a high-amplitude burst at 1:10 on October 2. d) Tremor bursts on August 5 during the 2018EW jökulhlaup, including the highest amplitude bursts recorded. Located tremor bursts are denoted by their origin in the eastern (E) and western (W) cauldrons. See figure 13. – *Tromlurit, tíðnisíuð frá 0,5 til 4 Hz, af stöðugum óróa (a) og óróahviðum (b,c,d) sem einkenna seinni fasa Skaftárhlaupa. Tromluritin eru af lóðrétta (HHZ) skjálftanema skjálftamælisins á Dyngjujökli (DJK), sem er staðsettur um 15 km austnorðaustan við eystri ketilinn og um 20 km austan við vestari ketilinn (1. mynd). a) Viðvarandi, sterkur órói frá kl. 16:00–18:00 þann 4. ágúst, í jökulhlaupum úr báðum kötlunum samtímis, 2018EW. b) Óróahviður 2.–3. september í jökulhlaupinu 2021W. Stöðugur órói fylgdi í kjölfar sterkrar óróahviðu rétt fyrir miðnættið. c) Óróahviður 1.–2. október i jökulhlaupi 2015E, úr eystri katlinum. Sterkasta hviðan varð kl. 01:10 þann 2. október. d) Óróahviður 5. ágúst í jökulhlaupunum 2018EW. Sterkustu hviðurnar hafa verið staðsettar, þær fyrri koma frá eystri katlinum (E), síðan tekur vestari ketillinn (W) við um hádegið. Sjá einnig 13. mynd.*

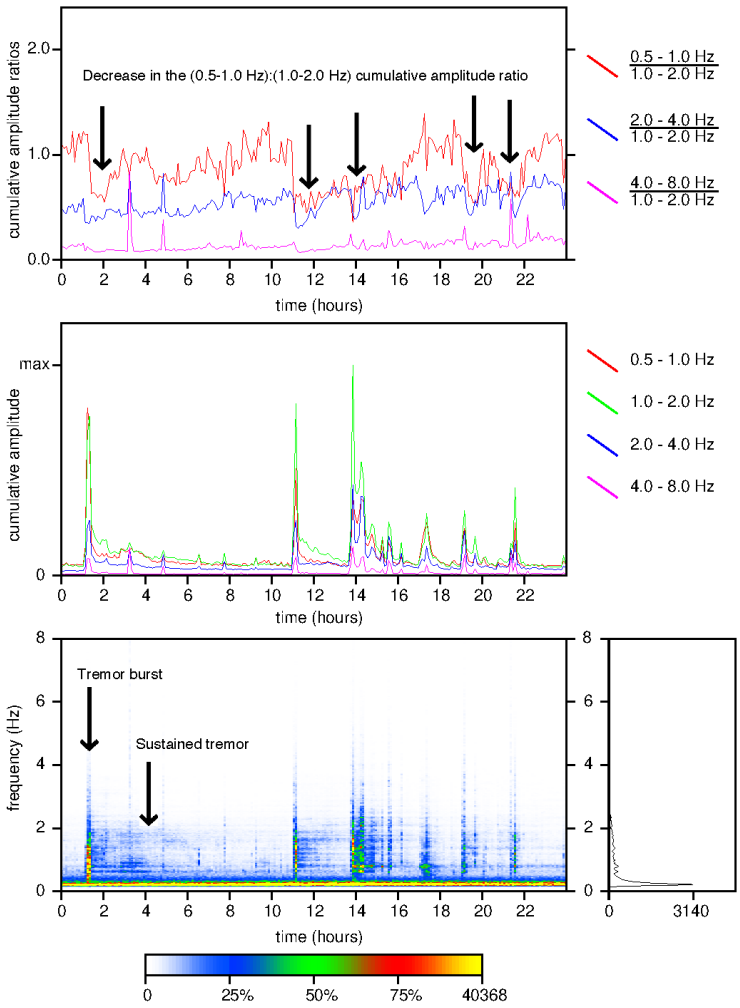

Figure 11. Spectral characteristics of Phase II tremor bursts starting on October 2nd during the 2015E jökulhlaup (Figure 10b), showing the vertical component of station DJK. Cumulative amplitude ratios (top), cumulative amplitude spectral density (middle), and spectrograms with linear amplitude scaling (bottom). – *Tíðnieinkenni óróatoppa 2. október 2015 í seinni fasa jökulhlaups 2015E, á lóðrétta nema skjálftamælisins á Dyngjujökli (DJK). Tíðnirit (neðst), styrkur óróans mældur sem tegur útslagsrófsins yfir tiltekin tíðnibil (í miðju) og hlutföll styrksins á tilteknum tíðnibilum (efst). Stöðugur óróa er áberandi í nokkrar klukkustundir í kjölfar óróahviðanna, dregur niður styrkinn á lægstu tíðnunum (efst).*

hlaups. Most of the seismic energy is focused below 1.2 Hz (Figure 11), with an exponential increase in spectral amplitude towards lower frequencies, which are obscured by the ocean induced microseisms. A reasonable estimate of the lower frequency bound can be obtained by examining the phase coherence of the tremor, as opposed to using single-station spectrograms. At most seismic stations during these small jökulhlaups, slightly inflated spectral amplitudes persist until 4 Hz, containing low-amplitude spectral lines. During larger jökulhlaups, including the 2015E, 2018EW, and 2021WE jökulhlaups, the sustained tremor has a wider frequency range and more distinct spectral lines (e.g. Figure 5) compared to those observed during smaller jökulhlaups.

The frequency content of the tremor is similar between larger jökulhlaups, exhibiting high spectral amplitudes from 0.2 Hz to 2.5 Hz and weaker, yet elevated, amplitudes up to 4 Hz at seismic stations within 25 km of the cauldrons, namely DJK, GRF, HUS, and VONK. As the distance between the cauldrons and a seismic station increases, higher frequencies are attenuated in the seismic record, and the spectral amplitude of the sustained tremor decreases. At the closest station, DJK, the most distinct spectral peaks occur between 0.75 and 1.25 Hz, but there are

many smaller peaks that occur throughout the active frequency range. For a single station during different large jökulhlaups, the dominant spectral peaks are typically very similar but not identical. During the two largest recent 2015E and 2018EW jökulhlaups, the spectral peaks of the sustained tremor are more distinct (Figures 5 and 11). Sustained tremor can be observed weakly at seismic stations as far as 40 to 60 km from the cauldrons.

Tremor bursts

Tremor bursts (0.5–4 Hz) begin several hours after the initiation of the sustained tremor. They can be distinguished from the sustained tremor based on their higher amplitude, shorter duration, and wider frequency content. Typically, these tremor bursts last an average of 12 minutes, ranging from 3 to 40 minutes in duration. Typically, between two and eleven bursts were clearly observed during each of the recent jökulhlaups. On average, there is usually a 3-hour delay between individual tremor bursts, but this interim time can fluctuate between 1 and 11 hours. These tremor bursts are observed across the western Vatnajökull seismic network, with a minimum range of 60 km from the cauldrons. High-amplitude tremor bursts during large jökulhlaups (e.g. the 2018EW jökulhlaup) can be observed as far as 150 km from the cauldrons.

Typically, the maximum seismic energy is not maintained throughout a tremor burst. Instead, several pulses of increased amplitude occur. Usually, 1–6 pulses of higher seismic energy comprise a single tremor burst as seen in Figure 12, which shows two individual tremor bursts that emerge with no clear phases in the waveform. The pulses have a higher frequency content than the sustained tremor and can reach up to 30 Hz, but the higher frequencies have lower spectral amplitudes and are only apparent with logarithmic spectral amplitude scaling. Typically, the maximum amplitudes with linear spectral amplitude scaling can reach as high as 8 Hz, but most energy is focused between 0.5 and 4 Hz.

The amplitude of the sustained tremor sometimes increases immediately after a tremor burst, and the frequency range of this background tremor temporarily widens for several hours (Figures 11 and 12c). The amplitude of sustained tremor is typically on the order of 10^{-6} m/s, which can be observed 40 km away from the cauldrons. However, following the particularly large tremor bursts observed during the 2015E, 2018EW, and 2021WE jökulhlaups, sustained tremor temporarily exhibits amplitudes on the order of 10^{-5} m/s, an order of magnitude larger, and can be observed at seismic stations 60 km from the cauldrons. This heightened amplitude can last for several hours, appearing to be a tail behind the tremor bursts (Figure 11). An examination of the frequency content of this tail at individual seismic stations reveals that it contains approximately the same frequency content and spectral lines as the sustained tremor that occurs before and during the tremor bursts.

During Phase II of the 2015E, 2019W, 2021W, and 2021E Skaftárhlaups, RSAM calculations averaged over 10 minutes reveal that the average velocity of ground motion for the largest tremor bursts is on the order of 10^{-5} m/s. Average amplitudes were an order of magnitude smaller for the 2015W jökulhlaup and an order of magnitude larger for the 2018EW jökulhlaup. Particularly large tremor bursts with amplitudes exceeding 10^{-4} m/s occur four times during the 2018EW jökulhlaup but only once during the 2015E, 2019W, and 2021W jökulhlaups. As the tremor period progresses for a single jökulhlaup, there is no pattern dictating when higher- versus lower-amplitude tremor bursts will occur. Amplitudes of the tremor bursts are highest at stations close to the cauldrons, decaying with distance. Energy is primarily lost in the vertical component by the time the tremor reaches further stations, manifesting relatively higher amplitudes in the eastern component of the seismogram. Nonetheless, most of the tremor bursts are large enough to be observed clearly at all stations around western Vatnajökull (Figure 1), both on and off of the glacier.

The tremor bursts, which generally exhibit phase coherence across the network within 0.3 and 10 Hz (Figure 9), exhibit a wider frequency content but are in the same part of the frequency domain as the sustained tremor, which typically exhibits phase coherence between 0.5 and 3 Hz. Although the tremor exhibits phase coherence over a wider range of frequen-

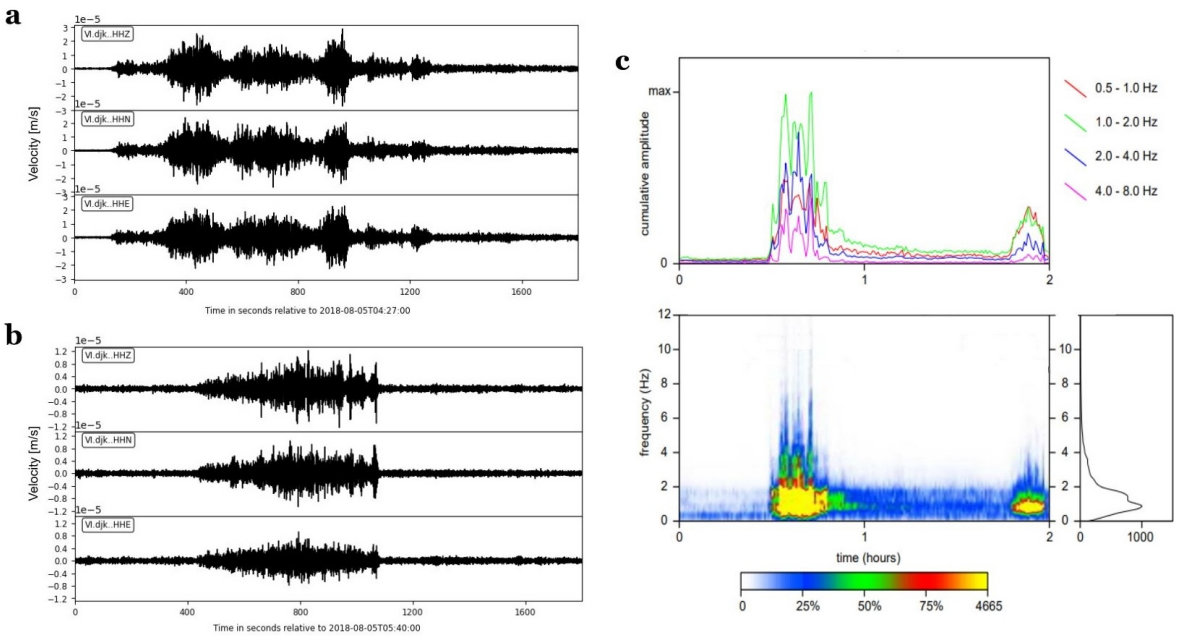

Figure 12. Two 30-minute-long waveforms and spectra of tremor bursts during the 2018EW jökulhlaup at DJK. a) Waveform of tremor on August 5 at 4:27. b) Waveform of the lower amplitude tremor on August 5 at 5:40. c) Cumulative amplitude spectral density (upper) and spectrogram with linear spectral amplitude scaling (lower) of the two tremor bursts at station DJK. The time axis ranges from 4:00–6:00 on August 5, 2018. – *Línurit og tíðniróf af 30 mínútna löngum óróahviðum í jökulhlaupinu 2018EW á þremur nemum (Z, N-S og A-V) skjálftamælisins á Dyngjujökli (DJK). a) Bylgjuform óróahviðu 5. ágúst klukkan 4:27. b) Bylgjuform óróahviðu með lægri sveifluvídd 5. ágúst klukkan 5:40. Sjá einnig 10. mynd. c) styrkur beggja hviða (ofar) og tíðniróf þeirra (neðar). Tímaásinn er frá 4:00–6:00 þann 5. ágúst 2018.*

cies, this is not representative of the dominant and highest amplitude frequencies of the tremor, which remain strongest from 0.5–4 Hz for the tremor bursts and 1–3 Hz for the sustained tremor, visualized by spectrograms. The 2015W tremor bursts have a narrower range of phase coherence, from 0.6-5 Hz, and the 2018EW tremor has a broader range, with phase coherence exceeding 10 Hz in the upper limit.

When a tremor burst occurs, there is a sharp change in the cumulative amplitude ratios between the 0.5–1.0 Hz frequency band and the 1.0–2.0 Hz frequency band (Figures 5 and 11). Tremor bursts during most jökulhlaups exhibit an instantaneous sharp drop in the (0.5–1.0 Hz):(1.0–2.0 Hz) ratio, indicating a drastic relative increase in the 1.0–2.0 Hz frequency range (e.g. Figure 11). A similar pattern is sometimes observed between the (2.0–4.0 Hz):(1.0–2.0 Hz) and the (4.0-8.0 Hz):(1.0–2.0 Hz) ratios, but it is less clear, less drastic, and less consistent than the change in the (0.5–1.0 Hz):(1.0–2.0 Hz) ratio. Once a tremor burst ceases, the cumulative spectral density ratio does not automatically return to its pre-burst ratio. Instead, the (0.5–1.0 Hz):(1.0–2.0 Hz) ratio slowly increases until another tremor burst occurs, indicating that the strong 1.0–2.0 Hz frequencies are fading after the tremor burst. This general pattern is observed by all stations in western Vatnajökull for a single tremor event, regardless of the station's distance from the cauldrons. In contrast to this typical activity, it should be noted that several of the largest tremor bursts during the 2018EW jökulhlaup exhibit a sharp spike, not drop, in the (0.5–1.0 Hz):(1.0–2.0 Hz) ratio (Figure 5). This relative increase in frequencies between 0.5 and 1.0 Hz occurs during three of the

largest tremor bursts with RSAM amplitudes exceeding 10^{-4} m/s. Similarly, the first few tremor bursts during the 2021E jökulhlaup exhibit a spike in the (0.5–1.0 Hz):(1.0–2.0 Hz) ratio, before transitioning to a drop in the ratio for subsequent tremor bursts.

Tremor burst location

The most prominent tremor bursts of the 2015–2021 Skaftárhlaups were located using the probabilistic methodology of Li and Gudmundsson (2020). Results show that the tremor bursts are located at the Skaftá cauldrons, typically near or within the boundary of the active cauldron that has just drained and produced a jökulhlaup (Figure 13). The quality of the location, judged by the width of the probability distribution, is generally better when more stations are used in the calculation and when the signal-to-noise ratio is higher. The large tremor bursts on August 5, during the 2018EW jökulhlaup, move between the cauldrons, which drained within 24 hours of one another. The first two bursts (Figure 13a-b), originate at the eastern cauldron, which was the first cauldron to drain. The next several bursts, which exhibit the highest amplitudes out of all tremor bursts observed during the 2015–2021 Skaftárhlaups, are located at the western cauldron (Figure 13c-d), which drained one day after the eastern cauldron. The locations vary slightly between consecutive tremor bursts located at a single cauldron (Figure 13). Despite the sparse seismic network, most tremor bursts are clearly located at either cauldron, thus associating each with a given cauldron. Several exceptions arise where the tremor is unexpectedly located near the inactive cauldron. The durations of the tremor bursts with this strange behavior were generally shorter than average, which could potentially lead to unstable results. Additionally, residual signals from local or regional earthquakes may contaminate the results.

DISCUSSION AND INTERPRETATION

Phase I: Seismic signals from propagating water

The transient seismic signals that occur during the main period of flood propagation and cauldron subsidence are related to the rapid propagation of the subglacial flood wave. The brief, low-amplitude transients are interpreted as icequakes generated by cracking as the glacier shifts and as hydrofracturing in the ice. The low-frequency, repetitive events, which typically cluster in time and space and exhibit a rhythmic pattern, are interpreted as stick-slip events at the glacier bed.

Generation of icequakes

The small, spatially incoherent transient signals are interpreted as icequakes that are produced by strain exerted on the glacier by the propagating flood wave. As a subglacial pressure wave advances during a fast-rising Skaftárhlaup, the glacier is rapidly lifted as high as 1 m off the bedrock to accommodate subglacial sheet-like flow (Jóhannesson, 2002; Björnsson *et al.*, 2003, 2010; Einarsson *et al.*, 2016; Eibl *et al.*, 2023). Einarsson *et al.* (2016) report that temporary horizontal displacement is also recorded at the glacier surface as the flood wave passes. The high frequency icequakes occurring during the Skaftárhlaups are likely generated by cracking as the ice experiences vertical and horizontal displacement, this observation is supported by the lack of phase coherence, the very small amplitudes, and the simple waveforms. Similar icequakes have been observed during a fast-rising jökulhlaup from the A. P. Olsen Ice Cap in NE-Greenland, which Behm *et al.* (2020) infer to be associated with the creation of surface crevasses. However, large surface crevasses have not been observed above the subglacial flood path of the Skaftárhlaups. Heightened levels of basal water along the subglacial flood path may increase basal sliding, which can in turn lead to increased seismicity and crevassing in response to faster ice stream flow (Behm *et al.*, 2020; Eibl *et al.*, 2023). Large, near-concentric crevasses form around the cauldrons during their subsidence. Using data from two seismic arrays in addition to the local seismic network, Eibl *et al.* (2023) located icequakes around the eastern cauldron and along the flood path, as the subglacial pressure wave propagated along the glacier bed during the 2015E Skaftárhlaup.

Although crevasses typically form near the glacier surface where the pressure is lower and the ice can easily undergo brittle deformation, they are not necessarily confined to near surface depths. While ele-

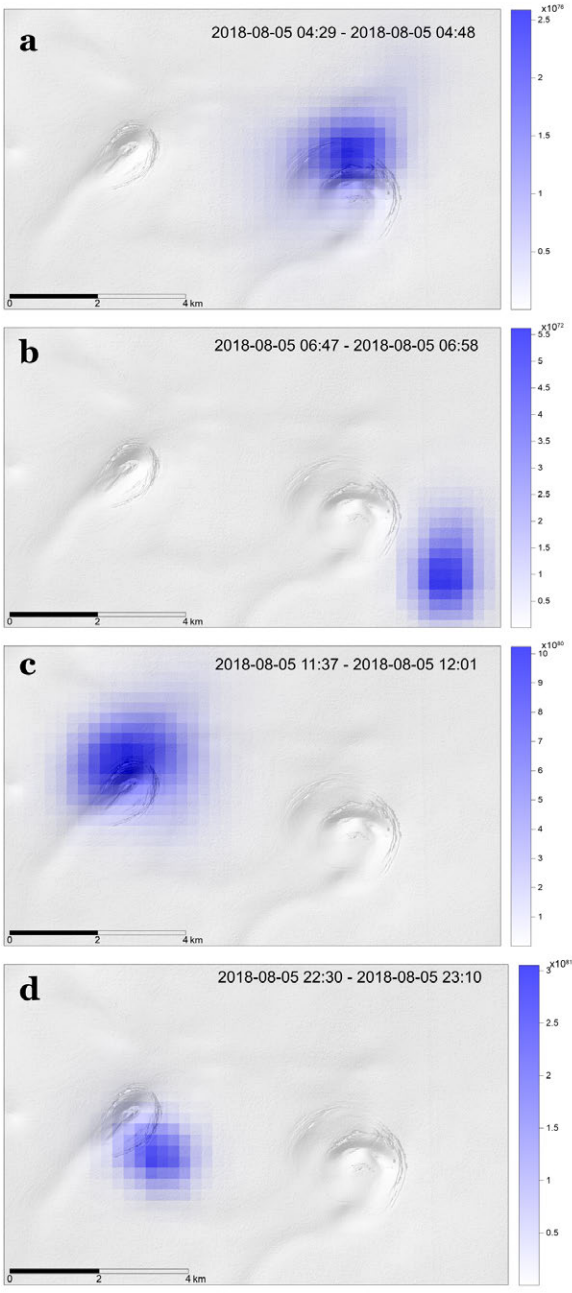

Figure 13. Probabilistic locations of four of the largest tremor bursts on August 5 during the 2018EW jökulhlaup. Locations are plotted on a DEM of the ice surface of the cauldrons. – *Líklegasta staðsetning fjögurra stærstu óróahviðanna 5. ágúst í jökulhlaupinu 2018EW á korti af yfirborði Skaftárkatlanna.*

vated meltwater levels can extend surface crevasses down to the bedrock through hydrofracturing (van der Veen, 1998, 2007), hydro-fractures can also originate near the base of the glacier and propagate upwards towards the glacier surface during fast-rising jökulhlaups (Bennett *et al.*, 2000; Roberts *et al.*, 2000). Some icequakes during the Skaftárhlaups may therefore be related to hydrofracturing in response to the high basal water pressure, not only the creation of surface crevasses as the glacier lifts. Bennett *et al.* (2000) and Roberts *et al.* (2000) present evidence that subglacial water may have leaked onto the glacier surface during the 1991 jökulhlaup-induced surge of Skeiðarárjökull, which is approximately 40 km ESE of Skaftárjökull. Floodwater may similarly create a superficial outlet atop the glacier during Skaftárhlaups, during which basal pressure may be so high that englacial drainage channels are fed or generated through hydrofracturing, creating some of the small, frequent icequakes that are observed. Basal crevasses have been detected by GPR during the fast-rising jökulhlaup from the A. P. Olsen Ice Cap in NE-Greenland, which created fractures up to the ice surface near the glacier terminus (Behm *et al.*, 2020). Based on this behavior during other fast-rising jökulhlaups, it is possible that icequakes during the Skaftárhlaups represent a mixture of basal hydraulically-induced fractures and surface crevasses.

Generation of low-frequency events

The low-frequency, repetitive transient signals that fall into the 0.5–3 Hz frequency range are likely associated with a repetitive basal process such as hydraulic jacking, basal sliding, or stick-slip movement (e.g. Danesi *et al.*, 2007; Podolskiy and Walter, 2016; Walter *et al.*, 2013; Wiens *et al.*, 2008; Winberry *et al.*, 2009). These repetitive events do not arise during all jökulhlaups, only occurring clearly during the 2018EW, 2019W, and 2021WE jökulhlaups.

The similarity in waveforms of the cluster of repeating low-frequency events on August 4 during the 2018EW jökulhlaup (Figures 6 and 10a) indicates that they are generated by a shared mechanism and spatially close. Well-constrained locations from Winder *et al.* (2021) confirm that the repetitive events during the 2018EW flood are clustered in the same location, but further analysis must be conducted to verify if this is also true for the 2019 and 2021 Skaftárhlaups. The striking waveform similarity of these events renders them suitable for detailed relative relocation (e.g. Sgattoni *et al.* 2016a; Sgattoni *et al.* 2016b), which could resolve this.

Bedrock topography at the location of the 2018 events begins to decrease in elevation from 700–800 m down to 600–700 m, entering the valley to the east of the ridge between Tungnaárjökull and Skaftárjökull (Björnsson and Pálsson, 2020). At the southwest margin of probable event locations, a hill exceeding 700 m elevation splits this entrance to the valley. One interpretation is that these low-frequency events are generated by floodwater lifting the glacier via hydraulic jacking as it encounters the hill as an obstacle. Sheet-like flow from the Skaftá cauldrons is susceptible to irregularities in the thickness of the sheet, so conduits with tunnel-like flow may form where the melt-rate ability, which describes how much energy is available in the floodwater to melt ice from the channel walls (Magnússon *et al.*, 2011), of the conduit is positive (Einarsson *et al.*, 2016). When subglacial floodwater encounters an adverse bed slope, the pressure melting point of the ice is affected and the water may supercool due to a lack of heat generation, creating a pooling of water above the adverse bed slope where the formation of efficient conduits cannot occur (Magnússon *et al.*, 2011). This may lift the glacier sharply with the arrival of a subglacial pressure wave, which causes the pressure to rise very quickly and then drop, inducing abrupt basal sliding events with a stick-slip motion at the same location with similar waveforms, produced by the repeating mechanism. The occurrence of this behaviour is based on the melt-rate ability of the channel walls (Magnússon *et al.*, 2011). The timing of these events usually occurs as the last of the water flows out of the cauldron, which may be explained by the floodwaters having a more difficult time overcoming the adverse bed slope in the case of stick-slip events caused by hydraulic jacking, due to less water pressure at the end of the jökulhlaup.

Stick-slip events beneath the David Outlet Glacier in East Antarctica are clustered in space, show high waveform similarity, and have similar magnitudes

(Danesi *et al.*, 2007). Observations of low-frequency events along the Skaftárhlaup flood path share these characteristics, suggesting they may also be stick-slip events, possibly involving hydraulic jacking. Basal stick-slip earthquakes with very long periods (20–150 seconds) have been identified at the Whillans Ice Stream in West Antarctica, exhibiting high waveform similarity (Wiens *et al.*, 2008). These events are much larger (magnitude M > 4) than Skaftarhlaup events (M < 1, based on IMO locations and unpublished Cambridge data), although both may reflect similar processes. Increased basal meltwater, especially during summer, raises normal stresses at asperities (Gräff and Walter, 2021), enhancing the likelihood of seismic stick-slip events during Skaftárhlaups. Similar phenomena have also been linked to jökulhlaups from Katla (Sgattoni *et al.*, 2016b).

The waveforms of the low-frequency Skaftárhlaup events slightly evolve from one event to the next (Figure 8a). An analogue may be drawn between this behavior and that of gliding tremor, which can be observed during repetitive periodic slip-failure of a single small asperity (Wiens *et al.*, 2008) and during changing geometry of a subglacial resonating crevasse (Helmstetter *et al.*, 2015). It is possible that the gradual changes in the waveform of the low-frequency Skaftárhlaup events result from slow changes in the geometry of the source at the bedrock.

Phase II: Tremor related to bedrock unloading

Phase II of a Skaftárhlaup, which begins after the cauldrons have undergone most drainage and subsidence, is dominated by 1.5–3 days of seismic tremor located at the cauldrons. Based on the 2015–2021 jökulhlaups, this tremor must be related to the rapid depressurization and destabilization of the bedrock and geothermal systems underlying the cauldrons, facilitating vigorous hydrothermal or volcanic activity (Figure 14).

Consideration of hydrothermal sources

Phase II tremor may be related to hydrothermal processes, initiated by the rapid decompression of the lakebed and underlying aquifer (Figure 14a). Vigorous geothermal boiling has been observed following the rapid depressurization of other subglacial systems, including jökulhlaups from Grímsvötn when the drop in water level reaches 10–30 m (Einarsson *et al.*, 2023). This geothermal tremor is characterized by its relatively high frequency (2–6 Hz) and oscillating amplitudes. It remains for a period after all water has been drained from the caldera lake. This type of tremor is seldom recorded beyond the edge of the glacier. Einarsson *et al.* (2023) suggest that the geothermal tremor is generated by flash-boiling of the geothermal system within the caldera, triggered by the pressure drop of the lake level. With the relief of overburden pressure, geothermal fluids may boil in-situ or rise to the surface (Smith and McKibbin, 2000). Alternatively, the pressure drop may allow magma at depth to shift and rise in the bedrock below the cauldrons, increasing heat in the aquifer and initiating vigorous boiling.

The geothermal nature of the aquifers beneath the Skaftá cauldrons likely affects the permeability and strength of the host rock, priming it for instability and making it more susceptible to triggers that may cause explosive hydrothermal activity (Montanaro *et al.*, 2022). Sealing via mineralization, pre-explosive boiling, or magma movement may further destabilize the aquifer after depressurization from the jökulhlaup. As discussed by Montanaro *et al.* (2022), cyclical pressurization and fracturing can enhance fluid circulation in shallow layers of a hydrothermal system, increasing instability and explosive risk. At the Skaftá cauldrons, which experience drastic, nearly sustained pressurization from meltwater accumulation and semi-annual periods of rapid depressurization, the underlying instability of the geothermal systems and potential repeated hydrothermal explosions may form a positive feedback loop.

The seismic signatures of the Skaftárhlaup tremor bursts share many similarities with tremor coinciding with hydrothermal explosive unrest at other sites worldwide, including White Island in New Zealand (Ardid *et al.*, 2022; Caudron *et al.*, 2018), Bogoslof volcano in Alaska (Searcy and Power, 2020), Kusatsu-Shirane volcano in Japan (Yamada *et al.*, 2021), Mt. Ontake in Japan (Caudron *et al.*, 2022a), and Lascar volcano in Chile (Gaeta *et al.*, 2020). Tremor during many of these events exhibits a dominant frequency

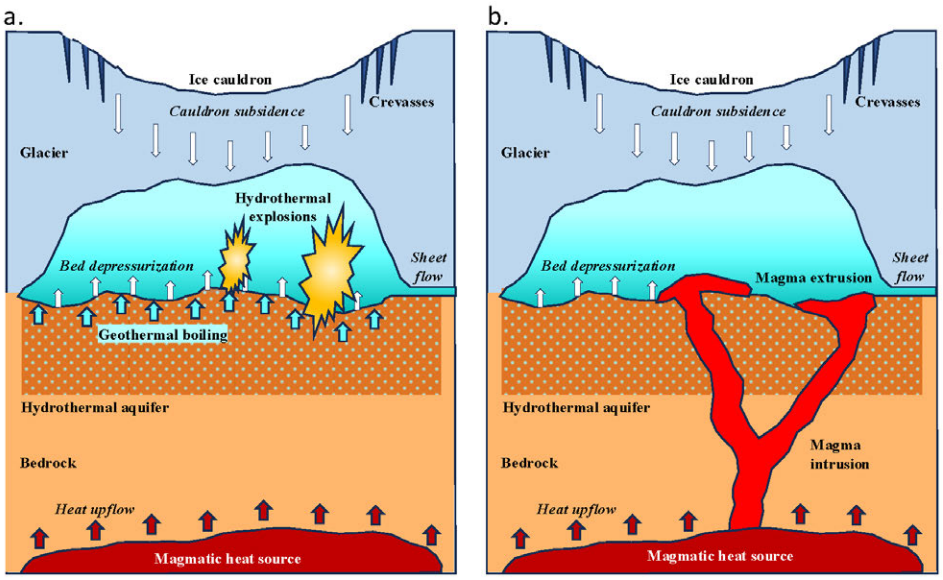

Figure 14. Conceptual models showing the proposed hypotheses of strong tremor generation during Phase II of a Skaftárhlaup. a) Conceptual Model One – Hydrothermal sources, including geothermal boiling (sustained tremor) and hydrothermal explosions (tremor bursts); b) Conceptual Model Two – Possible magmatic sources, including magma intrusions (tremor bursts) and extrusions (sustained tremor). It is possible that a combination of the potential hydrothermal and magmatic source processes illustrated here are occurring to generate the strong Phase II tremor. – *Skýringarmyndir af tilgátum um uppruna óróa og sterkra óróahviða í seinni fasa Skaftárhlaupa. a) Jarðhitalíkan gerir ráð fyrir að óróinn tengist suðu í jarðhitakerfinu vegna snöggrar þrýstingslækkunar við það að vatnið rennur frá kötlunum; b) Kvikulíkan gerir ráð fyrir að óróahviðurnar tengist kvikuhreyfingum í rótum háhitakerfisins vegna þrýstingslækkunarinnar og að lítill hluti kvikunnar geti hugsanlega náð til yfirborðs undir kötlunum.*

content from 1-10 Hz, generally with the strongest frequencies up to 4 Hz (Caudron *et al.*, 2018, 2022a; Gaeta *et al.*, 2020; Searcy and Power, 2020). The shape of the seismic envelope of the Skaftárhlaup tremor bursts, which is characterized by amplitude modulations and a heightened tail of lower amplitude sustained tremor, is similarly seen during hydrothermal explosions and phreatic eruptions (e.g. Gaeta *et al.*, 2020). At the Lascar volcano, this tremor was accompanied by a visible explosive plume and a degassing pulse (Gaeta *et al.*, 2020), exhibiting a tremor burst followed by a tail of comparatively lower amplitude harmonic-appearing tremor. In 2013, a series of small hydrothermal explosions occurred following a jökulhlaup from the ice-dammed Kverkfjöll lake, Gengissig, which is located approximately 45 km northeast of the Skaftá cauldrons (Montanaro *et al.*, 2016). The largest explosion, which was quite small and brief compared to the high-amplitude and long duration tremor bursts from the Skaftá cauldrons, had dominant frequencies from 0.5–2.5 Hz and weaker frequencies up to 4 Hz, with a faint tail of elevated tremor. While some of these features resemble the Skaftárhlaup tremor bursts, the amplitude of the largest explosion was on the order of 3000 nm/s, or 3×10^{-6} m/s (Montanaro *et al.*, 2016), which is two orders of magnitude smaller than the amplitudes of the largest Skaftárhlaup tremor bursts.

Hydrothermal explosions can produce craters with diameters from several meters to 2 km, with depths from several to hundreds of meters (Browne and Lawless, 2001; Muffler *et al.*, 1971). At Gengissig, craters up to 24 meters in diameter were measured (Montanaro *et al.*, 2016). Geothermally active crater-like de-

pressions less than 0.5 km in length were identified in the bedrock below the eastern Skaftá cauldron by Magnússon *et al.* (2021) via radio-echo soundings, reflecting areas where plumes of convective heat flow preferentially melt the ice overhead and expand the subglacial lake. Active geothermal vents which may change between years (Magnússon *et al.*, 2021), produce an upwelling of heat, representing possible locations for hydrothermal explosive activity.

There is evidence that geothermal fluids may be ejected from significant depths beneath the Skaftá cauldron geothermal systems. Forty percent of the total volume of the subglacial lakes has infiltrated into the bedrock below the cauldrons (Guðmundsson *et al.*, 2018), and a chemical analysis of the western Skaftá cauldron lake revealed that it includes a component of geothermal fluid originally from a depth with temperatures of 300°C (Jóhannesson *et al.*, 2007). This may be facilitated by an initial deep-sourced hydrothermal explosion that breaks through a seal or cap rock and causes soft sediments to collapse into the crater, continually increasing pressure and triggering frequent explosions. This type of activity was observed by Gallagher *et al.* (2020) at Champagne Pool, Wai-o-tapu, New Zealand, but more information about local sediments would be needed to link this type of mechanism to the Skaftá cauldrons seismic unrest.

Consideration of magmatic tremor sources

An alternative explanation is that the tremor is related to magmatic source processes such as magmatic intrusions or small subglacial eruptions in response to rapid bedrock depressurization (Figure 14b). Magma may migrate to shallower depths in response to rapid decompression of the bedrock, potentially enhancing hydrothermal activity or resulting in the extrusion of magma. Such an eruption may be effusive, as strong tremor does not necessarily indicate that explosive activity is occurring, as illustrated by a sudden increase in tremor marking the transition from explosive to effusive activity during the 2010 Eyjafjallajökull eruption (e.g. Benediktsdottir *et al.*, 2022; Caudron, *et al.*, 2022b). Furthermore, Einarsson and Brandsdóttir (1984) note that there is a correspondence between the rate of extrusion and the amplitude of tremor, but that an explosive eruption does not necessarily have a higher extrusion rate than an effusive eruption.

This hypothesis of tremor generation by subglacial volcanic processes is supported by the substantial distance from the cauldrons at which the tremor can be observed. The sustained tremor travels up to 60 km, while high-amplitude tremor bursts can be observed up to 150 km from the source, a similar scale on which eruption tremor from other Icelandic volcanoes is observed (Einarsson, 2018). The Skaftá cauldrons are located within the Eastern Volcanic Zone and surrounded by subglacial volcanic structures and central volcanic complexes (Björnsson and Einarsson, 1990), so it is very possible that similar processes occur beneath the Skaftá cauldrons and cause small, short-lived intrusions or extrusions of magma. Low frequency tremor is associated with non-eruptive magma movement (e.g. at Sakurajima volcano, Japan, Permana *et al.*, 2021). Additionally, Eibl *et al.* (2020) identify that the tremor occurring after cauldron subsidence is comprised of body waves, which may support the hypothesis of a tremor source at depth due to magma migration below the geothermal system.

Similar tremor accompanied the 2011 jökulhlaup from Katla, one of the most hazardous subglacial volcanoes in Iceland (Sgattoni *et al.*, 2017). In addition to flood tremor, this episode of unrest produced low-frequency volcanic or hydrothermal tremor from 0.8–4 Hz located near the active ice cauldrons. The latter tremor is reminiscent of tremor located at the Skaftá cauldrons, consisting of sustained tremor and distinct tremor bursts. The sustained tremor continues for 23 hours, causing a general drop in the cumulative amplitude ratio between 0.5–1.0 Hz and 1.0–2.0 Hz, indicating stronger frequencies between 1.0 and 2.0 Hz are present during the tremor. The tremor bursts, which have durations of several minutes, vary widely in amplitude and rise above the amplitude of the sustained tremor, as seen during the Skaftárhlaup tremor. Sgattoni *et al.* (2017) offer two potential interpretations of this tremor, favoring the prior: 1) a minor subglacial eruption that caused rapid melting of the glacier, or 2) purely hydrothermal processes involving boiling and/or hydrothermal explosions triggered

when the flood began to drain from the cauldron. Like the Skaftá cauldrons, Katla is overlain by a glacier, so it is impossible to directly observe any explosive, magmatic, or hydrothermal activity that occurred during any episode of unrest that is not significant enough to break through the overlying ice.

Out of all Icelandic volcanoes, Grímsvötn exhibits the highest eruption frequency (Þórarinsson, 1974). The sustained tremor and tremor bursts share many similarities with low-frequency volcanic tremor in Iceland, including eruptive tremor at Grímsvötn, as described by Einarsson and Brandsdóttir (1984), who identified two classes of volcanic tremor during the 1983 subglacial eruption of Grímsvötn: background tremor and tremor bursts. These two types of tremor are reminiscent of those observed at both the Skaftá cauldrons and at Katla in 2011 (Sgattoni et al., 2017). The background tremor, which was most intense during the first 12 hours of the 1983 Grímsvötn eruption, but persisted for several days, had a monochromatic character, exhibiting a fairly consistent amplitude. Tremor bursts with varying amplitudes and durations started a few hours later, exhibiting strong bursts for the first day that subsequently decreased in strength and continued for an additional 2.5 days (Einarsson and Brandsdóttir, 1984). While spectral characteristics were difficult to discern in the analog seismic records of the time, Einarsson and Brandsdóttir (1984) determined that the background tremor usually has a predominant frequency below 3 Hz, while the tremor bursts had predominant frequencies that fluctuated between 2 and 5 Hz. Both types of tremor, which were observed at significant distances from Grímsvötn, are associated with the volcanic eruption (Einarsson and Brandsdóttir, 1984).

By comparing tremorplots of the Grímsvötn jökulhlaups in 2008 and 2010, and the Grímsvötn eruptions in 2004 and 2011, Einarsson et al. (2023) identified three types of tremor: Water flood tremor, geothermal tremor, and eruption tremor. Water flood tremor at 2–9 Hz is associated with jökulhlaups from the Grímsvötn caldera, which are initiated when the lake level begins to drop and increase gradually with increasing water discharge from the lake. This tremor is usually detected a few days before the subglacial flood reaches the glacier edge. Geothermal tremor (2–6 Hz) appears to be switched on when the drop in water level of the caldera lake reaches 10–30 m, and remains after all water has been drained from the lake. This tremor is characterized by its relatively high frequency and abrupt amplitude oscillations. The geothermal tremor is considered to be generated by flash-boiling of the geothermal system within the caldera, triggered by the pressure drop of the lake level. It is seldom recorded beyond the edge of the glacier. Eruptions of Grímsvötn are accompanied by 0.5–4 Hz eruption tremor that begins simultaneously with the eruption outbreak and is distinctly different from the other two types of tremor based on its lower frequencies and wider distance range. It is recorded beyond the edge of the glacier.

If tremor bursts coinciding with the end of Skaftárhlaups represent a series of small, cyclical subglacial intrusions or eruptions, questions arise about the nature of volcanism beneath the Skaftá cauldrons. Unlike other volcanoes in the rift zone beneath Vatnajökull, which often exhibit long-term precursory activity and reliable short-term activity during dike propagation leading up to an eruption (Einarsson, 2018), the Skaftá cauldrons exhibit low-levels of seismicity. The apparent absence of significant earthquake activity at the Skaftá cauldrons differs from what is commonly observed at contemporary basaltic rift volcanoes in Iceland, such as Grímsvötn and Krafla (Einarsson and Brandsdóttir, 1984; Einarsson, 2018). This discrepancy may be explained by a non-basaltic volcanic structure beneath the Skaftá cauldrons, driven by a periodic relief of overlying pressure. Additionally, frequent eruptive activity leads to smaller eruptions (Marzocchi and Zaccarelli, 2006), indicating that the high frequency of jökulhlaups from the Skaftá cauldrons may facilitate numerous small extrusive events instead of large, easily-observed eruptions.

Evaluating the hypothesized tremor generation mechanisms

The origin of the strong tremor episodes observed during Skaftárhlaups remains uncertain, though several mechanisms can be hypothesized. Geothermal

boiling is expected following the rapid depressurization of subglacial geothermal areas, but this raises a question: How strong can the seismic source of geothermal activity be? At geothermal areas such as Svartsengi and Ölkelduhals (e.g. Brandsdóttir *et al.*, 1994; Gudmundsson and Brandsdóttir, 2010), low-amplitude sustained tremor is facilitated by gentle, near-surface boiling, which could be a weak source compared to the hypothesized scenario of confined hydrothermal activity occurring at hundreds of meters of depth following rapid depressurization of the geothermal area underlying the Skaftá cauldrons. The confined environment beneath the glacier makes it impossible to assert exactly which mechanisms and conditions must be met to generate the apparent strength of this tremor. The Skaftárhlaup tremor bursts were two orders of magnitude stronger in amplitude than those produced by the Gengissig hydrothermal explosions (Montanaro *et al.*, 2016), which were not large compared to other examples and were coupled poorly into seismic energy because they were surficial and poorly confined. The question becomes if this could explain the two orders of magnitude difference between the highest amplitudes of the largest Gengissig and Skaftárhlaup tremor bursts. Additionally, the Skaftárhlaup tremor bursts were of considerably longer duration than the Gengissig tremor burst following a single explosion, up to tens of minutes versus tens of seconds. If the short duration of individual hydrothermal explosions at Gengissig is also characteristic of such explosions in a confined environment, then a series of cascading explosions at Skaftá cauldrons must be inferred.

The strong tremor episodes following Skaftárhlaups may alternatively be generated by magmatic processes, such as shallow intrusions or even extrusions, triggered by the rapid depressurization of the subglacial lakebed and underlying geothermal system. These tremor bursts share striking similarities with seismic signals associated with small subglacial effusive eruptions, such as those at nearby Grímsvötn (Einarsson *et al.*, 2023) and other volcanic systems (e.g, Benediktsdottir *et al.*, 2022), including comparable frequency ranges and sufficient energy to propagate tens of kilometers above background noise levels. While these similarities are not conclusive evidence, they align with the hypothesis that volcanic activity may be the source of the tremor. The clear association between tremor at Grímsvötn and local volcanic activity strengthens this interpretation, but uncertainties remain regarding the precise physical mechanisms involved, the depth of the source, and factors affecting propagation. However, the possibility of subglacial geothermal activity producing tremor with similar features, as observed at the Skaftá cauldrons and Katla in 2011 (Sgattoni *et al.*, 2017), cannot be excluded, highlighting the need for further investigation into the conditions required to generate tremor of this magnitude and spectral signature.

Implications of electrical conductivity measurements

The secondary rise in electrical conductivity (Figure 3) recorded at Sveinstindur is directly related to the strong seismic tremor that begins approximately one day prior. This timing corresponds to the expected travel time of water from the cauldrons to the gauging station once the subglacial flood path has been created, indicating that the secondary increase in conductivity is related to the tremor generation mechanism, located at the cauldrons. The primary increase in conductivity that rises with the initial flood wave remains elevated once it reaches a local maximum value, indicating that the initial conductivity increase represents the baseline conductivity of the geothermally heated water from the subglacial lake. In contrast, the secondary spike in conductivity begins to decrease immediately once the maximum value is reached, suggesting that it was caused by a short-lived process such as the upwelling of geothermal fluids (e.g. Kataoka *et al.*, 2019) or interaction between magma and the geothermal fluids (e.g. Gaillard and Marziano, 2005). Decompression is a driving or triggering factor of the tremor observed at the Skaftá cauldrons, as there is a direct correlation between the unloading of the lakebed and tremor bursts located at the cauldrons. A strong positive relationship exists between the maximum of the secondary electrical conductivity spike and the maximum tremor burst RSAM, further solidifying the causality of the secondary conductivity spike by the source of tremor.

A positive relationship exists between the magnitude of a jökulhlaup, judged by its maximum discharge rate, and the maximum amplitude of the tremor. This relationship is not as well correlated as that of tremor amplitude and conductivity, but it is clear that larger jökulhlaups with higher flow rates and deeper cauldron subsidence generally yield stronger tremor. A strong positive correlation does exist between maximum conductivity and maximum flood discharge, which can be looked to as a proxy for the relationship between tremor amplitude and flood magnitude. While a larger pressure decrease (i.e. more cauldron subsidence and lake drainage) can facilitate stronger tremor with a higher amplitude, it does not directly constrain the duration of tremor bursts. The speed at which pressure is alleviated and the total vertical lake level drop does not always affect the size of the tremor bursts. The 2019W jökulhlaup, which propagated slowly resulted in 40–50 m less cauldron subsidence than the large 2015E and 2018EW jökulhlaups, is an outlier; it had a maximum tremor amplitude on the same order of magnitude as observed during the largest jökulhlaups, which experienced significantly higher subsidence and corresponding pressure relief. Disregarding the uncharacteristic 2019W jökulhlaup, the higher magnitude jökulhlaups typically do have higher amplitude tremor than smaller magnitude jökulhlaups.

Drilling into the western Skaftá cauldron in 2003 (Jóhannesson *et al.*, 2007) and both cauldrons in 2015 (Gaidos *et al.*, 2020) revealed that both subglacial lakes include a component of geothermal fluids, associated with high-temperature geothermal activity. Because the subglacial processes of tremor generation cannot be directly observed, water samples of proglacial discharge can help to reveal the true picture. Old *et al.* (2005) and Eibl *et al.* (2023) collected water samples during Skaftárhlaups. These studies agree that water samples contain a component of geothermal fluid. Eibl *et al.* (2023) report that water samples from the large 2015E jökulhlaup contain elevated concentrations of inorganic carbon, which indicates that the water spent a prolonged period of time interacting with rock before it was exposed subaerially. High boron concentrations additionally indicate that the reservoir grew beneath the ice cauldron gradually and had prolonged reactions with the bedrock before the 2015E jökulhlaup (Eibl *et al.*, 2023). Old *et al.* (2005) state that the fine particle size of suspended sediments during the 1997 Skaftárhlaups is consistent with that of sediment mobilized by rising steam from hydrothermal processes. Water samples indicate that upwelling from the geothermal system does occur in some capacity, whether this is related to vigorous geothermal boiling, hydrothermal explosions, or a combination of the two (Eibl *et al.*, 2023; Old *et al.*, 2005).

Distinct chemical signatures of uniquely volcanic components can be difficult to discern in water samples. While Eibl *et al.* (2023) did not find evidence of interactions between magma and the sampled water, Old *et al.* (2005) identified peaks in chloride and fluoride, which may be derived from the volcanic degassing of HCl and HF from magma (Sigurðsson *et al.*, 1985). Magma migration may be occurring in the bedrock below the cauldrons, possibly enhancing hydrothermal processes due to increased heat or resulting in small eruptions.

SUMMARY AND CONCLUSIONS

Between 2015 and 2021, the Skaftá cauldrons produced a total of eight jökulhlaups, three from the eastern cauldron and five from the western cauldron. During these floods, the cauldrons deepen as water rushes beneath Vatnajökull ice cap into the Skaftá river. Skaftárhlaups exhibit a wide variety of seismic activity, ranging from small icequakes to strong tremor, with a timeline of activity that remains quite similar between jökulhlaups.

Seismic activity begins during Phase I of a Skaftárhlaup shortly before the cauldron noticeably subsides, continuing until the cauldron has almost completely subsided and drained. While the flood propagates subglacially, transient signals dominate the seismic record. Based on network covariance matrix analysis, no tremor is coherently observed across the seismic network in western Vatnajökull during this phase. The first class of transients during Phase I are small, localized signals that do not exhibit phase

coherence. They are interpreted as icequakes created by hydrofracturing and ice deformation when the subglacial floodwave lifts the overlying glacial ice. They are frequent but very short in duration, lasting from a fraction of a second to several seconds. Their small amplitudes do not facilitate spatial coherence for most of these signals, which may explain why tremor observed by Eibl *et al.* (2020, 2023) during floodwater propagation was not identified by network covariance matrix analyses. The second class of transients during this phase of a Skaftárhlaup are repetitive, low-frequency events that typically cluster in time, exhibiting very similar waveforms and a rhythmic pattern, occurring every 0.5–2 hours. These signals are interpreted as basal stick-slip events, possibly generated when the floodwater encounters an adverse bed slope.

Phase II of a Skaftárhlaup is dominated by strong tremor. Sustained tremor that is strongest from 1–3 Hz begins once most of the water has drained from the cauldrons and continues for 1.5 to 3 days. It exhibits phase coherence across western Vatnajökull and initiates as a weak signal of limited frequency range, expanding after several hours to include higher and lower spatially coherent frequencies, ranging from 1–4 Hz for the smaller jökulhlaups and 0.7–5 Hz for the larger 2015E and 2018EW jökulhlaups. Distinct spectral lines persist throughout the period of sustained tremor without deviation, but these spectral peaks are not at the same frequencies at all seismic stations during a given event. This must therefore be a propagation effect rather than a source characteristic. Higher frequencies are attenuated at seismic stations farther from the cauldrons. During the larger 2015E and 2018EW jökulhlaups the amplitude of the sustained tremor is higher, allowing for a wider range of frequencies to travel across the network, above the noise level.

Tremor bursts that are enriched in intermediate frequencies (strongest from 0.5–4 Hz) and have durations from several minutes to 10s of minutes begin after sustained tremor initiates. The amplitudes of tremor bursts are larger than the sustained tremor, and they are observed by seismic stations as far as 150 km from the cauldrons. Typically, several clear bursts occur in the days following a Skaftárhlaup, with a several hour delay between individual bursts. This tremor is spatially coherent across the network, exhibiting phase coherence from 0.3–10 Hz for most jökulhlaups. The spectral content is similar at individual stations between bursts of similar amplitudes, but the spectral peaks do exhibit variations, as higher frequencies are attenuated at stations farther from the cauldrons. The frequency content of a tremor burst is directly associated with the amplitude of the tremor burst, with larger bursts containing a wider range of frequencies. The maximum seismic energy is not maintained during a single tremor burst and is instead spasmodic and modulated by a series of pulses of increased amplitude. These tremor bursts are sometimes trailed by a faint tail of tremor with heightened amplitudes that can last for several hours, having the same spectral characteristics and peaks as the sustained tremor.

The origin of the strong tremor episodes during Skaftárhlaups remains uncertain, though several mechanisms can be hypothesized. Geothermal mechanisms such as enhanced boiling and possibly hydrothermal explosions are expected following the rapid depressurization of geothermal areas, but it is important to consider how strong the seismic source of geothermal activity can be. While the apparent strength of tremor at the Skaftá cauldrons is high, it is important to consider that this tremor is possibly being generated at a significant depth beneath the cauldrons. The tremor shares characteristics with seismic signals that are associated with subglacial volcanism, including small subglacial eruptions at Grímsvötn, such as comparable frequency ranges and long-range propagation, supporting the hypothesis of a volcanic origin. However, uncertainties about the physical mechanisms, source depth, and factors affecting propagation highlight the need for more detailed research into the conditions required to generate tremor of this magnitude and spectral signature.

A relationship exists between the magnitude of a jökulhlaup in terms of discharge and the maximum amplitude of tremor bursts. Tremor bursts with amplitudes on the order of 10^{-4} m/s have been recorded at both the eastern and western cauldrons, with the strongest tremor bursts between 2015 and 2021 oc-

curring within the western Skaftá cauldron during the 2018EW jökulhlaup. The maximum secondary rise in electrical conductivity recorded in the Skaftá river has a direct relationship with the maximum amplitude of the tremor bursts. This relationship warrants further investigation, as it could provide valuable insights into the complexities of subglacial geothermal environments.

A summary of our main findings is as follows:

1. Small, low-energy, short range, transient signals are interpreted as icequakes from hydrofracturing and ice deformation as the water starts to migrate subglacially.
2. Higher energy, longer range, repetitive events, possibly relating to stick-slip glacier motion at the bedrock, arise during the main phase of the jökulhlaup.
3. Sustained tremor (1–3 Hz) begins once most water has drained from the cauldron, persisting for 1.5–3 days.
4. High-amplitude tremor bursts (0.5-4 Hz), with durations up to tens of minutes and strong relationships with increased electrical conductivity of the water are observed once most of the water has drained from the cauldrons.
5. A probabilistic location method reveals that this 0.5–4 Hz tremor, which corresponds temporally to the end of cauldron subsidence, is co-located with the cauldrons, indicating that the tremor is related to the rapid depressurization of the bedrock. Based on its duration, amplitude and temporal correlation with a marked increase in suspended material in the Skaftá river, this tremor is likely related to confined shallow level magmatic activity or vigorous geothermal activity.
6. Based on the eight 2015–2021 jökulhlaups, the progression of seismic activity over the duration of the flood is similar, and there is a correspondence between flood magnitude and maximum tremor burst amplitude.

Acknowledgements

We gratefully acknowledge the assistance of Benedikt Ófeigsson and Tómas Jóhannesson, who coordinated the preparation of GPS data and Krista Hannesdóttir, for quick processing of this GPS data. We thank Þórdís Högnadóttir and Magnús Tumi Guðmundsson for providing their spreadsheet of cauldron subsidence data, collected through various methods. This information was vital to the holistic overview of the recent Skaftárhlaups. We thank Finnur Pálsson for generating the map on Figure 1. The IS-Tremor/IS-Noise research team who include some of the leading experts in the field of tremor analysis, offered significant insights into our data analyses methods. Thanks should also go to the Cambridge University scientists, who shared seismic data and location analyses. We thank our editor, Þorsteinn Þorsteinsson, and two anonymous reviewers for revisions which substantially improved the paper.

ÁGRIP

Skjálftavirkni samfara jökulhlaupum úr Skaftárkötlum, 2015–2021

Skaftárkatlar eru sigkatlar í vestanverðum Vatnajökli, norðvestan Grímsvatna. Slíkir sigkatlar myndast þar sem öflug jarðhitasvæði bræða þykkan jökulís. Jarðhitavatn safnast saman við botn jökulsins. Vatnsþrýstingur vex með tímanum vegna hækkandi vatnsstöðu, þar til vatnið brýst undan viðkomandi katli, rennur til suðvesturs 35–40 km undir jökulinum og kemur fram við upptök Skaftár í Skaftárhlaupum, á 1–5 ára fresti. Á jarðskjálftamælum má greina jarðhitasuð, smáskjálfta og sterkar óróahviður í jökulhlaupunum, sem hingað til hefur reynst erfitt að skilgreina. Með margþættri úrvinnslu gagna af fjölda jarðskjálftamæla frá átta jökulhlaupum á árunum 2015–2021, ásamt samanburði við GNSS-gögn og vatnshæðarmælingar, kemur í ljós að smáskjálftavirknin tengist útbreiðslu og farvegi jökulhlaupsins á afmörkuðu svæði við jökulbotninn, þar sem ætla má að vatnið mæti fyrirstöðu þegar það brýtur sér leið undir jöklinum. Hringlaga sigsprungur myndast í yfirborði jökulsins samhliða vatnsrennsli úr viðkomandi jarðhitakatli. Jökulhlaupunum fylgir hækkandi jarðórói í þá 1,5–3 sólarhringa sem þau standa. Þessi tegund óróa kemur fram á nálægum stöðvum og er talinn tengjast snöggri þrýstingslækkun og suðu í jarðhitakerfinu undir kötlunum og hugsanlega tengslum við grunnstæð kvikuinnskot sem kynda jarðhitakerfin. Sterkar óróahviður í tugi

mínútna koma fram á mælum á stærra svæði þegar líður á hlaupið og mest af vatninu hefur runnið úr kötlunum. Marktæk hækkun á leiðni í Skaftá tengist þessum óróahviðum, sem hafa upptök við katlana og verða sennilega vegna einhvers konar gufusprenginga, mögulega vegna kvikuhreyfinga í tengslum við þrýstingslækkun í jarðhitakerfinu.

REFERENCES

Ardid, A., D. Dempsey, C. Caudron and S. Cronin 2022. Seismic precursors to the Whakaari 2019 phreatic eruption are transferable to other eruptions and volcanoes. *Nature Comm.* 13(1). https://doi.org/10.1038/s41467-022-29681-y

Behm, M., J. I. Walter, D. Binder, F. Cheng, M. Citterio, B. Kulessa, K. Langley, P. Limpach, S. Mertl and W. Schöner 2020. Seismic characterization of a rapidly-rising jökulhlaup cycle at the A. P. Olsen Ice Cap, NE-Greenland. *J. Glaciology* 66(256), 329–347. https://doi.org/10.1017/jog.2020.9

Benediktsdóttir, Á., Ó. Gudmundsson, B. Brandsdóttir and A. Tryggvason 2017. Ambient noise tomography of Eyjafjallajökull volcano, Iceland. *J. Volc. Geotherm. Res.* 347, 250–263. https://doi.org/10.1016/j.jvolgeores.2017.09.017

Benediktsdóttir, Á., Ó. Gudmundsson, K. L. Li and B. Brandsdóttir 2022. Volcanic tremor of the 2010 Eyjafjallajökull eruption. *Geophys. J. Int.* 228(2), 1015–1037. https://doi.org/10.1093/gji/ggab378

Bennett, M. R., D. Huddart and R. I. Waller 2000. Glaciofluvial crevasse and conduit fills as indicators of supraglacial dewatering during a surge, Skeiðarárjökull, Iceland. *J. Glaciol.* 46(152), 25–34. https://doi.org/10. 3189/172756500781833232

Björnsson, H. 1988. *Hydrology of Ice Caps in Volcanic Regions.* Soc. Sci. Islandica, U. Iceland, 139 pp.

Björnsson, H. and P. Einarsson 1990. Volcanoes beneath Vatnajökull, Iceland: Evidence from radio echo-sounding, earthquakes and jökulhlaups. *Jökull* 40, 147–168. https://doi.org/10.33799/jokull1990.40.147

Björnsson, H. 2003. Subglacial lakes and jökulhlaups in Iceland. *Global and Planetary Change* 35(3–4), 255–271. https://doi.org/10.1016/s0921-8181(02)00130-3

Björnsson, H. 2010. Understanding jökulhlaups: From tale to theory. *J. Glaciol.* 56(200), 1002–1010. https://doi.org/10.3189/002214311796406086

Björnsson, H. and F. Pálsson 2020. Radio-echo soundings on Icelandic temperate glaciers: history of techniques and findings. *Ann. Glaciology* 61(81), 25–34. https://doi.org/10.1017/aog.2020.10

Brandsdóttir, B., P. Einarsson, K. Árnason and H. Kristmannsdóttir 1994. *Smáskjálfta- og bylgjubrotsmælingar í tengslum við niðurdælingu affallsvatns í jarðhitasvæðið við Svartsengi sumarið 1993.* (In Icelandic with an English abstract). Science Institute and National Energy Authority Joint Report RH03-94, OS94016/JHD-05, 28 pp.

Browne, P. and J. Lawless 2001. Characteristics of hydrothermal eruptions, with examples from New Zealand and elsewhere. *Earth-Science Rev.*, 52(4), 299–331. https://doi.org/10.1016/s0012-8252(00)00030-1

Böðvarsson, R., S. T. Rögnvaldsson, R. Slunga, and E. Kjartansson 1999. The SIL data acquisition system – at present and beyond year 2000. *Phys. Earth Planet. Inter.* 113, 89–101. https://doi.org/10.1016/S0031-9201(99)00032-1

Gaidos, E., T. Jóhannesson, B. Einarsson, Th. Thorsteinsson, J. P. Amend and M. Skidmore 2020. Après nous, le déluge: A human-triggered jökulhlaup from a subglacial lake. *Geophys. Res. Lett.* 47, e2020GL089876. https://doi.org/10.1029/2020GL089876

Caudron, C., B. Taisne, J. Neuberg, A. D. Jolly, B. Christenson, T. Lecocq, Suparjan, D. Syahbana, and G. Suantika 2018. Anatomy of phreatic eruptions. *Earth, Planets and Space* 70(1). https://doi.org/10.1186/s40623-018-0938-x

Caudron, C., Y. Aoki, T. Lecocq, R. De Plaen, J. Soubestre, A. Mordret, L. Seydoux and T. Terakawa 2022a. Hidden pressurized fluids prior to the 2014 phreatic eruption at Mt. Ontake. *Nature Comm.* 13(1). https://doi.org/10.1038/s41467-022-32252-w

Caudron, C., J. Soubestre, T. Lecocq, R. S. White, B. Brandsdóttir and L. Krischer 2022b. Insights into the dynamics of the 2010 Eyjafjallajökull eruption using seismic interferometry and network covariance matrix analyses. *EarthPlanet. Sci. Lett.* 585, 117502. https://doi.org/10.1016/j.epsl. 2022.117502

Danesi, S., S. Bannister and A. Morelli 2007. Repeating earthquakes from rupture of an asperity under an Antarctic outlet glacier. *Earth Planet. Sci. Lett.* 253(1–2), 151–158. https://doi.org/10.1016/j.epsl.2006.10.023

Eibl, E. P. S., C. J. Bean, B. Einarsson, F. Pálsson and K. S. Vogfjörd 2020. Seismic ground vibrations give advanced early-warning of subglacial floods. *Nature Comm.* 11(1). https://doi.org/10.1038/s41467-020-15744-5

Eibl, E. P. S., K. S. Vogfjörd, B. G. Ófeigsson, M. J. Roberts, C. J. Bean, M. T. Jones, B. H. Bergsson, S. Heimann and T. Dietrich 2023. Subaerial and subglacial seismic characteristics of the largest measured jökulhlaup from the eastern Skaftá cauldron, Iceland. *Earth Surf. Dynam.* 11, 933–959. https://doi.org/10.5194/esurf-11-933-2023

Einarsson, B. 2009. *Jökulhlaups in Skaftá: A study of jökulhlaup from the Western Skaftá cauldron in the Vatnajökull ice cap, Iceland.* VI-2009-006, report 90 pp. https://www.vedur.is/media/vedurstofan/utgafa/skyrslur/2009/VI_2009_006_tt.pdf

Einarsson, B., E. Magnússon, M. J. Roberts, F. Pálsson, Th. Thorsteinsson and T. Jóhannesson 2016. A spectrum of jökulhlaup dynamics revealed by GPS measurements of glacier surface motion. *Ann. Glaciology* 57(72), 47–61. https://doi.org/10.1017/aog.2016.8

Einarsson, B., T. Jóhannesson, Th. Thorsteinsson, E. Gaidos and T. Zwinger 2017. Subglacial flood path development during a rapidly rising jökulhlaup from the western Skaftá cauldron, Vatnajökull, Iceland. *J. Glaciol.* 63(240), 670–682. https://doi.org/10.1017/jog.2017.33

Einarsson, P., B. Brandsdóttir, M. T. Gudmundsson, H. Björnsson, K. Grönvold and F. Sigmundsson 1997. Center of the Iceland hotspot experiences volcanic unrest. *Eos, Transactions AGU* 78(35), 369. https://doi.org/10.1029/97eo00237

Einarsson, P. and B. Brandsdóttir 1984. Seismic activity preceding and during the 1983 volcanic eruption in Grímsvötn, Iceland (Skjálftavirkni tengd eldgosinu í Grímsvötnum 1983). *Jökull* 34, 13–23. https://doi.org/10.33799/jokull1984.34.013

Einarsson, P. 2018. Short-Term Seismic Precursors to Icelandic Eruptions 1973–2014. *Front. Earth Science* 6. https://doi.org/10.3389/feart. 2018.00045

Einarsson, P., F. Pálsson, M. Pálsson, E. Magnússon, B. Brandsdóttir and T. Winder 2023. Sources of continuous tremor associated with jökulhlaups and eruptions of Grímsvötn volcano, Iceland. *Jökull* 73, 55–74. https://doi.org/10.33799/jokull2023.73.055

Gaete, A., T. R. Walter, S. Bredemeyer, M. Zimmer, C. Kujawa, L. Franco Marin, J. S. Martin and C. Bucarey Parra 2020. Processes culminating in the 2015 phreatic explosion at Lascar volcano, Chile, evidenced by multiparametric data. *Nat. Hazards and Earth System Sci.* 20(2), 377–397. https://doi.org/10.5194/nhess-20-377-2020

Gaillard, F. and G. I. Marziano 2005. Electrical conductivity of magma in the course of crystallization controlled by their residual liquid composition. *J. Geophys. Res.* 20. https://doi.org/10.1029/2004JB003282

Galeczka, I., E. S. Eiriksdottir, J. Hardardottir, E. H. Oelkers, P. Torssander and S. R. Gislason 2015. The effect of the 2002 glacial flood on dissolved and suspended chemical fluxes in the Skaftá river, Iceland. *J. Volc. Geothermal Res.* 301, 253–276. https://doi.org/10.1016/j.jvolgeores.2015.05.008

Gallagher, A., C. Montanaro, S. Cronin, B. Scott, D. B. Dingwell and B. Scheu 2020. Hydrothermal eruption dynamics reflecting vertical variations in host rock geology and geothermal alteration, Champagne Pool, Wai-o-tapu, New Zealand. *Bull. Volc.* 82(77), 19 pp. https://doi.org/10.1007/s00445-020-01414-3

Gräff, D. and F. Walter 2021. Changing friction at the base of an Alpine glacier. *Sci. Rep.* 11(1). https://doi.org/10.1038/s41598-021-90176-9

Guðmundsson, M. T., E. Magnússon, Þ. Högnadóttir, F. Pálsson and C. Rossi 2018. Hættumat vegna jökulhlaupa í Skaftá. Skaftárkatlar – saga og þróun 1938–2018. *Hazard-assessment in connection with glacial outburst floods in the Skaftá river, development of the Skaftá cauldrons 1938–2018.* Raunvísindastofnun Háskólans RH-2018-16 og Veðurstofa Íslands VÍ 2018-017, 63 pp. [In Icelandic with and English abstract] https://www.vedur.is/media/vedurstofan-utgafa-2018/VI_2018_017_rs.pdf

Guðmundsson, Ó. and B. Brandsdóttir 2010. Geothermal noise at Ölkelduháls, SW Iceland. *Jökull* 60, 89–102. https://doi.org/10.33799/jokull2010.60.089

Helmstetter, A., L. Moreau, B. Nicolas, P. Comon and M. Gay 2015. Intermediate-depth icequakes and harmonic tremor in an Alpine glacier (Glacier d'Argentière, France): Evidence for hydraulic fracturing. *J. Geophys. Res.: Earth Surface* 120(3), 402–416. https://doi.org/10.1002/2014jf003289

Jakobsdóttir, S. S., G. B. Guðmundsson and R. Stefánsson 2001. Seismicity in Iceland 1991–2000 monitored by the SIL seismic system. *Jökull* 51, 87–94. https://doi.org/10.33799/jokull2002.51.087o

Jakobsdóttir, S. S. 2008. Seismicity in Iceland 1994–2007. *Jökull* 58, 75–100. https://doi.org/10.33799/jokull2008.58.075

Jóhannesson, T. 2002. Propagation of a subglacial flood wave during the initiation of a jökulhlaup. *Hydrological Sci. J.* 47(3), 417–434. https://doi.org/10.1080/02626660209492944

Jóhannesson, T., Th. Thorsteinsson, A. Stefánsson, E. J. Gaidos and B. Einarsson 2007. Circulation and thermodynamics in a subglacial geothermal lake under the Western Skaftá cauldron of the Vatnajökull ice cap, Iceland. *Geophys. Res. Lett.* 34(19). https://doi.org/10.1029/2007gl030686

Kataoka, K. S., T. Matsumoto, T. Saito, Y. Nagahashi and T. Iyobe 2019. Suspended sediment transport diversity in river catchments following the 2014 phreatic eruption at Ontake Volcano, Japan. *Earth, Planets and Space* 71(1). https://doi.org/10.1186/s40623-019-0994-x

Kristinsson, B. 2005. *Rennslismælingar í vestari kvísl Skaftár við vhm 470 og samanburður við rennsli Skaftár hjá Sveinstindi, vhm 166, árin 1997–2004.* National Energy Authority, report BK-2005/01. [In Icelandic]. http://www.os.is/gogn/Greinargerdir/Grg-OS-2005/BK-2005-01.pdf

Li, K. L. and O. Gudmundsson 2020. A Probabilistic Tremor Location Method. *Geophys. Res. Lett.* 47(4). https://doi.org/10.1029/2019gl085538

Magnússon, E., H. Rott, H. Björnsson and F. Pálsson 2007. The impact of jökulhlaups on basal sliding observed by SAR interferometry on Vatnajökull, Iceland. *J. Glaciol.* 53(181), 232–240. https://doi.org/10.3189/172756507782202810

Magnússon, E., H. Björnsson, H. Rott, M. J. Roberts, F. Pálsson, S. Gudmundsson, R. A. Bennett, H. Geirsson and E. Sturkell 2011. Localized uplift of Vatnajökull, Iceland: subglacial water accumulation deduced from InSAR and GPS observations. *J. Glaciol.* 57, 475–484. https://doi.org/10.3189/002214311796905703

Magnússon, E., F. Pálsson, M. T. Gudmundsson, Th. Högnadóttir, C. Rossi, Th. Thorsteinsson, B. G. Ófeigsson, E. Sturkell and T. Jóhannesson 2021. Development of a subglacial lake monitored with radio-echo sounding: case study from the eastern Skaftá cauldron in the Vatnajökull ice cap, Iceland. *The Cryosphere* 15(8), 3731–3749. https://doi.org/10.5194/tc-15-3731-2021

Marzocchi, W. and L. Zaccarelli 2006. A quantitative model for the time-size distribution of eruptions. *J. Geophys. Res.* 111(B4). https://doi.org/10.1029/2005jb003709

Montanaro, C., B. Scheu, M. T. Gudmundsson, K. Vogfjörd, H. I. Reynolds, T. Dürig, K. Strehlow, S. Rott, T. Reuschlé and D. B. Dingwell 2016. Multidisciplinary constraints of hydrothermal explosions based on the 2013 Gengissig lake events, Kverkfjöll volcano, Iceland. *Earth Planet. Sci. Lett.* 434, 308–319. https://doi.org/10.1016/j.epsl.2015.11.043

Montanaro, C., E. Mick, J. Salas-Navarro, C. Caudron, S. J. Cronin, J. M. de Moor, B. Scheuand, J. Stix and K. Strehlow 2022. Phreatic and Hydrothermal Eruptions: From Overlooked to Looking Over. *Bull. Volcanology* 84(6). https://doi. org/10.1007/s00445-022-01571-7

Muffler, L. J. P., D. E. White and A. H. Truesdell 1971. Hydrothermal Explosion Craters in Yellowstone National Park. *Geol. Soc. Am. Bull.* 82(3), 723. Retrieved from http://doi.org/10.1130/0016-7606(1971)82[723:heciyn]2.0.co;2

Murray, T. L. and E. T. Endo 1989. *A Real-time Seismic Amplitude Measurement system (RSAM).* U.S. Geological Survey Open-File Report 89-684, 21 pp. https://www.morageology.com/view_pub.php?id=311

Nye, J. F. 1976. Water Flow in Glaciers: Jökulhlaups, Tunnels and Veins. *J. Glaciology* 17(76), 181–207. https://doi.org/10.1017/s002214300001354x

Old, G. H., D. M. Lawler and R. Snorrason 2005. Discharge and suspended sediment dynamics during two jökulhlaups in the Skaftá river, Iceland. *Earth Surface Processes and Landforms* 30(11), 1441–1460. https://doi.org/10.1002/esp.1216

Permana, T., T. Nishimura, H. Nakahara and N. Shapiro 2021. Classification of volcanic tremors and earthquakes based on seismic correlation: application at Sakurajima volcano, Japan. *Geophy. J. Int.* 229(2), 1077–1097. https://doi.org/10.1093/gji/ggab517

Podolskiy, E. A., and F. Walter 2016. Cryoseismology. *Rev. Geophysics* 54(4), 708–758. https://doi.org/10.1002/2016rg000526

Roberts, M. J., A. J. Russell, F. S. Tweed and S. Knudsen 2000. Ice fracturing during jökulhlaups: implications for englacial floodwater routing and outlet development. *Earth Surface Processes and Landforms* 25(13), 1429–1446. https://doi.org/10.1002/1096-9837(200012)25:13<1429::AID-ESP151>3.0.CO;2-K

Searcy, C. K. and J. A. Power 2020. Seismic character and progression of explosive activity during the 2016–2017 eruption of Bogoslof volcano, Alaska. *Bull. Volc.* 82(1). https://doi.org/10.1007/s00445-019-1343-4

Seydoux, L., N. Shapiro, J. de Rosny, F. Brenguier and M. Landès 2016. Detecting seismic activity with a covariance matrix analysis of data recorded on seismic arrays. *Geophys. J. Int.* 204(3), 1430–1442. https://doi.org/10.1093/gji/ggv531

Sgattoni, G., Ó. Gudmundsson, P. Einarsson, F. Lucchi, K. L. Li, H. Sadeghisorkhani, R. Roberts and A. Tryggvason 2017. The 2011 unrest at Katla volcano: characterization and interpretation of the tremor sources. *J. Volc. Geotherm. Res.*, 338, 63–78. https://doi.org/10.1016/j.jvolgeores.2017.03.028

Sigurðsson, H., J. D. Devine and A. N. Davis 1985. The petrologic estimation of volcanic degassing. *Jökull* 35, 1–8. https://doi.org/10.33799/jokull1985.35.001

Smith T. A. and R. McKibbin 2000. An investigation of boiling processes in hydrothermal eruptions. *Proc. World Geothermal Congress 2000*, Tokyo, Japan (eds. E. Eglesias, D. Blackwell, T. Hunt, J. Lund, S. Tamanyu and K. Kimbora), (Int. Geothermal Ass. 2000, 699–704.

Soubestre, J., N. M. Shapiro, L. Seydoux, J. de Rosny, D. V. Droznin, S. Y. Droznina, S. L. Senyukov and E. I. Gordeev 2018. Network-Based Detection and Classification of Seismovolcanic Tremors: Example From the Klyuchevskoy Volcanic Group in Kamchatka. *J. Geophys. Res. Solid Earth* 123(1), 564–582. https://doi.org/10.1002/2017jb014726

Walter, F., J. F. Clinton, N. Deichmann, D. S. Dreger, S. E. Minson and M. Funk 2009. Moment tensor inversions of icequakes on Gornergletscher, Switzerland. *Bull. Seismol. Soc. Am.* 99(2A), 852–870. https://doi.org/10.1785/0120080110

Winder, T. E. B., C. Bacon, J. D. Smith, T. S. Hudson, J. Drew and R. S. White 2021. QuakeMigrate v1.0.0. Zenodo. https://doi.org/10.5281/zenodo.4442749

Wiens, D. A., S. Anandakrishnan, J. P. Winberry and M A. King 2008. Simultaneous teleseismic and geodetic observations of the stick–slip motion of an Antarctic ice stream. *Nature* 453(7196), 770–774. https://doi.org/10.1038/nature06990

Þórarinsson, S. 1974. *Vötnin stríð; Saga Skeiðarárhlaupa og Grímsvatnagosa.* (Swift Flowing Waters, the History of Floods in Skeiðará and Eruptions in Grímsvötn, in Icelandic). Bókaútgáfa Menningarsjóðs, Reykjavík, 254 pp.

van der Veen, C. 1998. Fracture mechanics approach to penetration of surface crevasses on glaciers. *Cold Regions Sci. Tech.* 27(1), 31–47. https://doi.org/10.1016/s0165-232x(97)00022-0

van der Veen, C. J. 2007. Fracture propagation as means of rapidly transferring surface meltwater to the base of glaciers. *Geophys. Res. Lett.* 34(1). https://doi.org/10.1029/2006gl028385

Yamada, T., A. K. Kurokawa, A. Terada, W. Kanda, H. Ueda, H. Aoyama, T. Ohkura, Y. Ogawa and T. Tanada 2021. Locating hydrothermal fluid injection of the 2018 phreatic eruption at Kusatsu-Shirane volcano with volcanic tremor amplitude. *Earth, Planets and Space* 73(1). https://doi.org/10.1186/s40623-020-01349-1

Zóphóníasson, S. and S. Pálsson 1996. *Rennsli í Skaftárhlaupum og aur- og efnastyrkur í hlaupum 1994, 1995 og 1996.* National Energy Authority, report OS96066/VOD-07. [In Icelandic]. http://www.os.is/gogn/Skyrslur/OS-1996/OS-96066.pdf